iScience

CellPress

Article

Low-Frequency Spike-Field Coherence Is a Fingerprint of Periodicity Coding in the Auditory Cortex

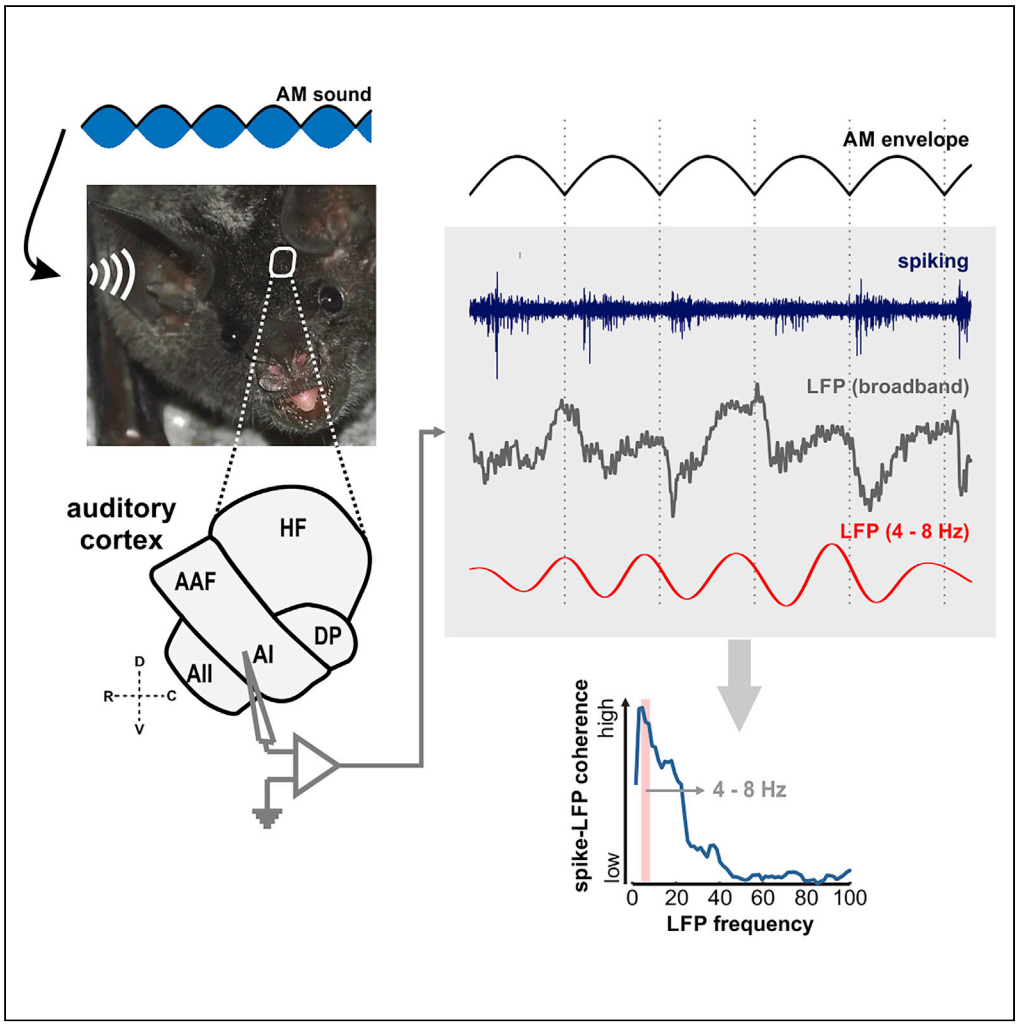

Francisco García-Rosales, Lisa M. Martin, M. Jerome Beetz, Yuranny Cabral-Calderin, Manfred Kössl, Julio C. Hechavarria

garciarosales@bio.uni-frankfurt.de (F.G.-R.)
hechavarria@bio.uni-frankfurt.de (J.C.H.)

HIGHLIGHTS

Auditory cortical neurons can track periodic sounds via synchronized spiking

Neuronal synchronization ability is well marked by theta-alpha spike-LFP coherence

Spike-LFP coherence patterns are independent of the stimulus' periodicity

Theta-alpha LFPs may orchestrate phase-locked neuronal responses to periodic sounds

García-Rosales et al., iScience 9, 47–62
November 30, 2018
https://doi.org/10.1016/j.isci.2018.10.009

iScience

CellPress

Article

Low-Frequency Spike-Field Coherence Is a Fingerprint of Periodicity Coding in the Auditory Cortex

Francisco García-Rosales,[1,5,*] Lisa M. Martin,[1] M. Jerome Beetz,[1,4] Yuranny Cabral-Calderin,[2,3] Manfred Kössl,[1] and Julio C. Hechavarria[1,*]

SUMMARY

The extraction of temporal information from sensory input streams is of paramount importance in the auditory system. In this study, amplitude-modulated sounds were used as stimuli to drive auditory cortex (AC) neurons of the bat species *Carollia perspicillata*, to assess the interactions between cortical spikes and local-field potentials (LFPs) for the processing of temporal acoustic cues. We observed that neurons in the AC capable of eliciting synchronized spiking to periodic acoustic envelopes were significantly more coherent to theta- and alpha-band LFPs than their non-synchronized counterparts. These differences occurred independently of the modulation rate tested and could not be explained by power or phase modulations of the field potentials. We argue that the coupling between neuronal spiking and the phase of low-frequency LFPs might be important for orchestrating the coding of temporal acoustic structures in the AC.

INTRODUCTION

The timing of acoustic events is of great importance to animals that rely on acoustic information for communication and/or orientation. It is known that the temporal structure of sounds carries relevant information for a variety of complex behaviors, including communication call processing (Drullman et al., 1994; Kanwal et al., 1994; Shannon et al., 1995; Theunissen and Doupe, 1998; Koch and Grothe, 2000) as well as navigation and spatial cues detection (Middlebrooks, 2015; Suga, 2015; Wohlgemuth et al., 2016). Ethologically relevant sounds usually occur in well-structured temporal patterns that ultimately facilitate their neuronal processing. A typical example of acoustic structures in nature is amplitude modulation (AM), which characterizes a wide variety of vocalizations (Luo et al., 2007; Arnal et al., 2015; Slama and Delgutte, 2015).

Amplitude-modulated sounds are acoustic signals composed of one or more carrier frequencies whose amplitudes vary as a function of a modulating wave. Sinusoidal amplitude modulations (modulating wave is a sine function) have been extensively used to investigate how the brain processes acoustic events (Rhode and Greenberg, 1994; Krishna and Semple, 2000; Lu et al., 2001; Joris et al., 2004; Yin et al., 2011; Niwa et al., 2015). The periodicity of AM sounds is encoded along the auditory pathway via a synchronized discharge of auditory neurons to a certain phase of the stimulus (phase code), or by increasing the firing rate as a response to an increase in the modulation frequencies (rate code) (Lu and Wang, 2000; Lu et al., 2001; Joris et al., 2004; Yin et al., 2011; Johnson et al., 2012). It is known that the capacity of neurons to produce phasic responses deteriorates in higher hierarchical structures of the auditory pathway (Joris et al., 2004). In the auditory cortex (AC) of several mammals, the neuronal synchronization ability is already limited to modulation rates not higher than ~35 Hz (Creutzfeldt et al., 1980; Schreiner and Urbas, 1988; Gaese and Ostwald, 1995; Fitzpatrick et al., 2009; Martin et al., 2017).

Although AM is a ubiquitous feature of natural sounds, how the mammalian AC processes amplitude envelopes is still not well understood. For example, most of the aforementioned studies focused on the encoding of the envelope's periodicity by cortical spike trains, but little is known about how other neuronal signals such as local-field potentials (LFPs, a slower component of the electrophysiological ensemble [Buzsaki et al., 2012]) are involved in the processing of AM stimuli. High-frequency oscillations of the LFPs are important for neural computations and attentional processes in sensory systems (Womelsdorf and Fries, 2007; Womelsdorf et al., 2007; Fries, 2009), whereas low-frequency fluctuations (typically <12 Hz) in cortical field potentials are associated with sensory selectivity (also linked to attention) and with the modulation of

[1]Institut für Zellbiologie und Neurowissenschaft, Goethe-Universität, Max-von-Laue-Str. 13, 60438 Frankfurt am Main, Germany

[2]MEG Labor, Brain Imaging Center, Goethe-Universität, 60528 Frankfurt am Main, Germany

[3]German Resilience Center, University Medical Center Mainz, Mainz, Germany

[4]Present address: Department of Zoology II, University of Würzburg, Am Hubland, Würzburg 97074, Germany

[5]Lead Contact

*Correspondence: garciarosales@bio.uni-frankfurt.de (F.G.-R.), hechavarria@bio.uni-frankfurt.de (J.C.H.)

https://doi.org/10.1016/j.isci.2018.10.009

neuronal excitability (Schroeder and Lakatos, 2009; Stefanics et al., 2010; Palva and Palva, 2011; Henry and Obleser, 2012; Ng et al., 2012). In the AC, it has been shown that stimulus-evoked spiking synchronizes to low-frequency (<12 Hz) fluctuations (Lakatos et al., 2005), and that such synchronization could be important for neuronal coding (Kayser et al., 2009) and predictive timing (Arnal and Giraud, 2012). However, evidence linking slow LFPs with the coding of periodic (and thus predictive) stimuli by auditory cortical neurons in the mammalian brain is lacking.

In this study, we aimed to bridge this gap by investigating how the AC of the bat *Carollia perscpicillata* processes AM sounds, considering spiking responses, LFPs, and their interactions in terms of their synchronization to the stimulus and to each other. Because of the evidence suggesting that slow oscillations play an important role in organizing cortical responses, we hypothesized that low-frequency coherence between spikes and LFPs would differ between neurons that phase lock to the AM envelope and those that do not. Our data confirmed this hypothesis. We show that the ability of phase coding periodic stimuli in the AC is marked by significant differences in the phase coherence of spikes and LFPs in the theta–alpha range (4–12 Hz). That is, coherence between both neural signals is strongest when neurons are able to track the periodicity of the stimulus in a phasic manner. Such strong spike-LFP coherence is observed even at modulation frequencies beyond the tracking limits of the cortical spiking. Overall, our data suggest an involvement of theta-alpha LFPs in orchestrating temporally organized neuronal firing to periodic acoustic streams.

RESULTS

Spiking Activity Synchronizes to Slow AM Stimuli

Cortical responses to AM sounds were recorded from 87 units in awake bats. Units were classified into two groups: trackers (showed significant phase synchronization to at least one modulation frequency) and non-trackers (were not significantly synchronized to any modulation rate). The phasic response of a typical tracker is depicted in the peri-stimulus time histogram (PSTH) shown in Figure 1A. This unit synchronized its discharge pattern to slow modulation frequencies, whereas it failed to do so to faster AM envelopes (>13.92 Hz). Note that the vector strength (VS) values calculated for the unit drop as the modulation frequency increases, as depicted in Figure 1C. The frequencies to which the unit was significantly synchronized, according to a "joint criterion" that includes both VS metrics and circular statistics (see Transparent Methods), are marked with red stars. Figure 1B shows the PSTH of a representative non-tracker, which failed to synchronize spikes to any modulation frequency tested. This unit did not fulfill the joint criterion for any of the presented stimuli (Figure 1D).

At the population level, 47.13% of the units were classified as trackers (41/87), whereas 52.87% (46/87) were classified as non-trackers. Tracking units showed high VS values for low modulation frequencies (Figure 1E, blue), with the tracking ability deteriorating in response to higher modulation rates. The subpopulation of trackers had significantly stronger VS than the subpopulation of non-trackers only when the modulation frequency was higher than 2 Hz, but lower than 13.92 Hz (false discovery rate [FDR]-corrected Wilcoxon rank-sum test; corrected $p \leq 0.0093$). Higher VS in trackers than in non-trackers is a consequence of the classification criterion (see Transparent Methods), but the fact that significant differences do not occur in response to rates above 13.92 Hz is also a sign of the deterioration of the tracking abilities with faster envelopes. To quantify the cortical phase-locking limits we defined, per unit, a modulation cutoff frequency representing the highest modulation rate to which the unit's spiking was significantly synchronized. Only a minority of the recorded units (10/87, 11.49%) were able to fire synchronously to AM envelopes faster than 22.63 Hz (Figure 1E), indicating that most cortical spiking could not follow rates higher than this value. Because of this, and based on the fact that most cortical phase coding responses across species occur at low modulation rates (see Joris et al., 2004), in the subsequent analyses we focused on tracking units whose cutoff frequency was not higher than 22.63 Hz (31 tracking units).

The existence of weak temporal organization in the response of a small number of non-tracking units was a possibility. In such cases, our approach would label these units as non-trackers, if their response patterns did not fulfill the classification criterion (see Transparent Methods). To explore the former, we considered pooled spiking responses from the group of trackers and non-trackers, per modulation frequency. We reasoned that if units in the AC synchronize to the same envelope phase for a given modulation rate (see Malone et al., 2007; Yin et al., 2011), pooled spikes across units could reveal the presence of (weak) temporal organization in the population response of non-trackers. Figure S1 shows pooled responses for the group of tracking and non-tracking units. The response of tracking units was well temporally organized, and spikes

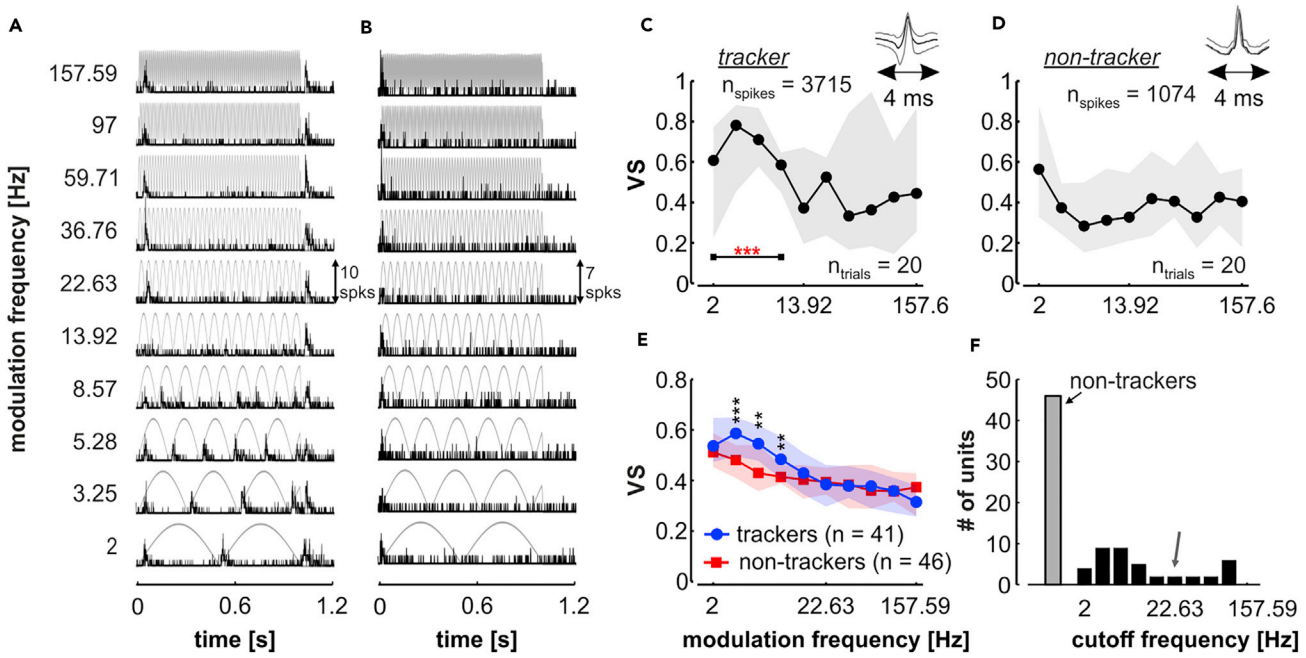

Figure 1. Tracking and Non-tracking Units in the AC of *C. perspicillata*

(A and B) Peri-stimulus time histograms (1-ms bins) of a cortical tracker (A) and a non-tracker (B).

(C) Vector strength (VS) of the tracking unit depicted in (A), for all modulation frequencies tested. This unit was significantly synchronized (according to the joint criterion, see Transparent Methods) to modulation frequencies up to 8.57 Hz (red stars).

(D) VS of the non-tracking unit shown in (B). Solid black lines in (C and D) represent the median VS across trials; gray-shaded areas illustrate the interquartile range (IQR). Waveforms on top of VS curves represent the spike shape of each unit (C, tracker, n = 3,715 spikes; D, non-tracker, n = 1,074 spikes; all spikes are included to obtain the waveform).

(E) Vector strength of tracking (blue circles) and non-tracking (red squares) units; solid lines show median values, whereas shaded areas indicate the IQR. (* symbols indicate the results of FDR-corrected Wilcoxon rank-sum tests; **p < 0.01, ***p < 0.001).

(F) Distribution of cutoff frequencies in the population of trackers (black bars; non-trackers represented by the gray bar). The gray arrow indicates a cutoff frequency of 22.63 Hz.

typically occurred at the same envelope phase across units, particularly in response to low modulation frequencies (Figure S1B). Importantly, pooled non-tracking responses still showed some temporal organization in their spiking, up to modulation rates of 13.92 Hz (note the circular spike-phase histograms in Figure S1C), which is in line with the idea that the definition of trackers and non-trackers is rather graded, and not strictly discrete. In addition, to evaluate to what extent the recorded units could overcome phase coding limitations to represent AM sounds, we quantified each unit's ability to encode the envelope's periodicity via a rate code, whereby a unit monotonically increases its firing rate in response to higher modulation frequencies. Although we observed rate coding responses in our data (see Figure S2), it was only in a minority of the population (13.79%, 12/87), comprising 14.63% of tracking (6/41) and 13.04% of non-tracking (6/46) units. Hence, we did not consider rate coding responses separately in further analyses.

Low-Frequency Spike-Field Coherence Is Strongest in Tracking Units

The spike-field coherence (SFC) metric was used to quantify differences between tracking and non-tracking units in terms of spike-LFP synchronization, across distinct frequency bands and modulation rates. In brief, the SFC is a normalized, frequency-dependent synchronization index that measures how well spikes lock to ongoing oscillations, by considering LFP windows related to the spiking activity. The value of the SFC in a certain frequency varies between 0 and 1, and it indicates the strength of the locking of spikes to that LFP frequency.

In tracking units, we observed that LFP segments centered at spike times typically carried strong slow oscillatory components, evidenced by the spike-triggered averages (STA; i.e., the average of the LFP segments associated to spikes; Figure 2A, black traces). Critically, such low-frequency components were not only

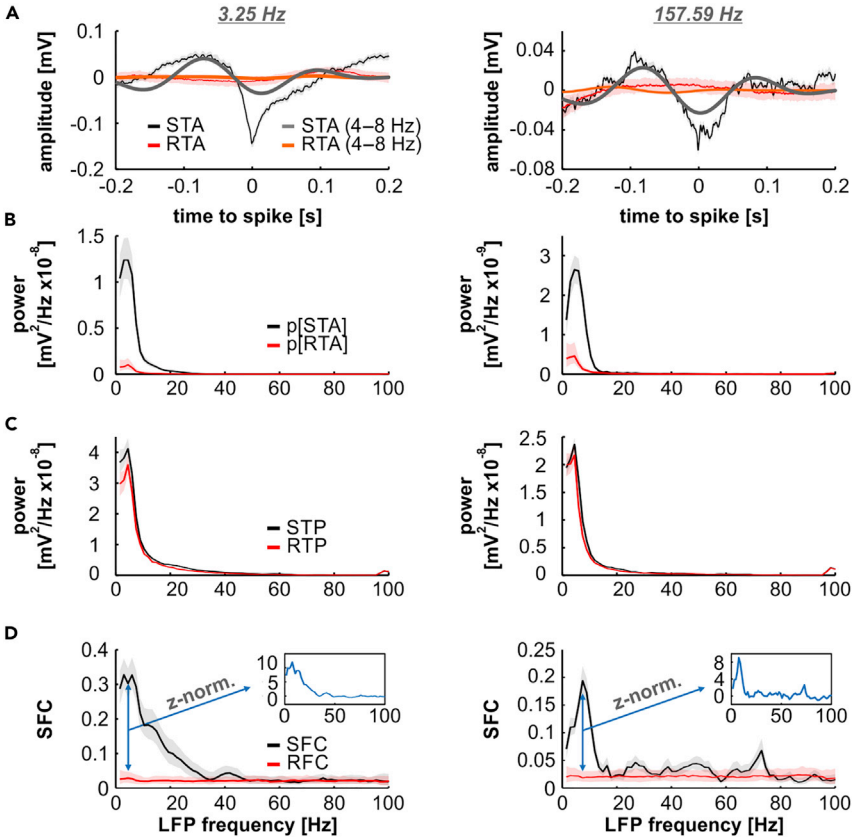

Figure 2. Spike-Field Coherence in an Exemplary Tracking Unit

(A) Left: Spike-triggered averages (STAs; solid lines: median; shaded areas: IQR) obtained from a representative tracker (same shown in Figure 1A) in response to a modulation frequency of 3.25 Hz. Dark traces show the STA calculated with real spike times (thin black curve, raw median STA; thick gray curve, 4–8 Hz filtered median STA, shown for illustrative purposes). Red and orange traces represent the raw median STA calculated with randomly centered LFP windows (random-triggered average [RTA]; red trace, raw median RTA; thick orange curve, 4–8 Hz filtered median RTA). Right: same as in left, but obtained in response to a modulation frequency of 157.49 Hz.

(B) Power spectral density of the STAs (black) and RTAs (red) obtained from data shown in (A) (left, 3.25 Hz; right, 157.59 Hz).

(C) Average power of the LFP windows centered at spike times (spike-triggered power [STP], black traces), and at random time points (random-triggered power [RTP], red traces). Left and right columns follow above-described conventions.

(D) Spike-field coherence (SFC, black traces) and random-field coherence (RFC, red traces), at two modulation frequencies (left column, 3.25 Hz; right column, 157.59 Hz). Insets show the z-normalization of the median SFC with respect to the RFC (baseline). Data in the figure are shown as median (solid lines) and IQR (shaded areas) across repetitions (300 in total) in the coherence analysis (See Transparent Methods).

present when the animals listened to slow AM envelopes (Figure 2A, left; modulation frequency of 3.25 Hz) but also appeared in response to modulation rates beyond the tracking ability of the cortical spiking (e.g., Figure 2A, right; modulation frequency of 157.69 Hz). The former implies that the presence of such slow fluctuations cannot be solely explained by separate entrainment of LFPs and spikes to the stimulus, since low-frequency LFPs would also not be phase locked to fast envelopes. Furthermore, if LFP segments were chosen at random time points and averaged (thus yielding the random-triggered average), the low-frequency oscillatory components considerably diminished in amplitude (red and orange traces in Figure 2A).

Coherence values were obtained after dividing the power of the STAs (Figure 2B) by the average power of the respective LFP segments (spike-triggered power; Figure 2C). The SFC of the example unit at two different modulation rates is depicted in Figure 2D (black trace). As a baseline, coherence was calculated using LFP windows chosen at random time points (red traces in Figure 2 depict data associated to randomly

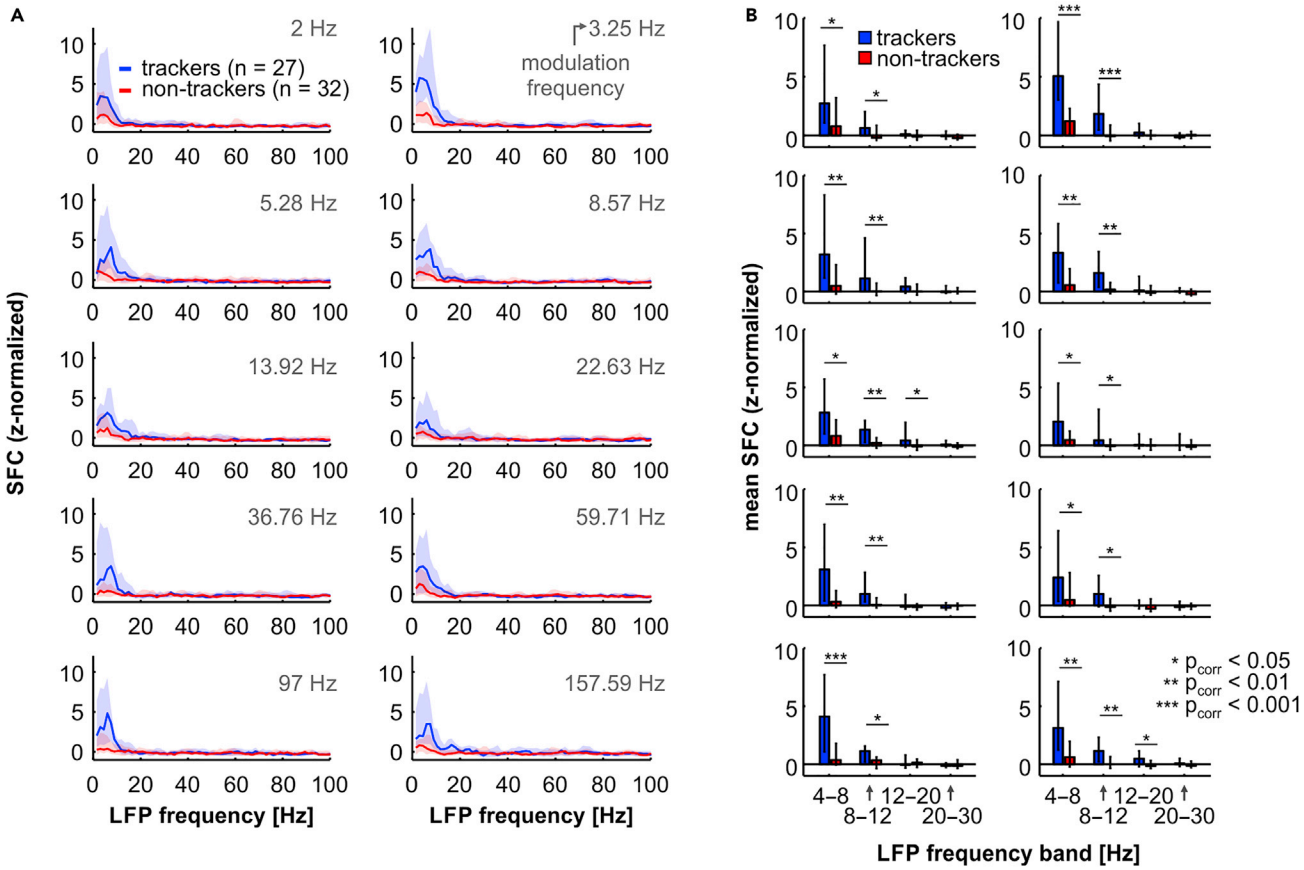

Figure 3. Theta-Alpha Spike-Field Coherence Is Strongest In Tracking Units across Modulation Frequencies

(A) z-normalized SFC across modulation frequencies (indicated in each sub-panel) in tracking (blue) and non-tracking units (red).

(B) Comparison, across modulation frequencies, of the average SFC in different LFP bands (theta, 4–8 Hz; alpha, 8–12 Hz; low beta, 12–20 Hz; and high beta, 20–30 Hz) in tracking (blue) and non-tracking (red) units. Each sub-panel shows the statistics for one modulation frequency; sub-panels are arranged as in (A). Data shown in the figure as median and 25th and 75th percentiles. Significance was assessed with FDR-corrected Wilcoxon rank-sum tests. All p values indicated in the figure are corrected for multiple comparisons. (* corrected $p < 0.05$; ** corrected $p < 0.01$; *** corrected $p < 0.001$).

selected LFP segments), which resulted in the "random-field coherence" (RFC; Figure 2D, red). The RFC represents spike-LFP synchrony obtained if consistent phase relationships between spikes and LFPs are absent. To allow for comparisons between units in further analyses, the median SFC across repetitions (within a unit and modulation frequency, see Transparent Methods) was z-normalized to the corresponding distribution of RFC values. The insets in Figure 2D show the normalized SFC for the exemplary tracking unit in response to low and high modulation rates (3.25 Hz, left; 157.59 Hz, right). Note that high SFC values are clearly present in both cases in low-frequency bands of the LFP.

Spike-field coherence was compared between the subpopulations of tracking and non-tracking units using the z-normalized SFC (illustrated in Figure 2D). Because the SFC is affected by the number of spikes (and hence the number of LFP windows) used to calculate it (Grasse and Moxon, 2010), we considered only units that fired at least 40 spikes in response to every modulation frequency presented. Thus, a total of 27 trackers and 32 non-trackers were used. Population z-normalized SFC values obtained from trackers and non-trackers, across modulation rates, are shown in Figure 3A (blue, trackers; red, non-trackers). In line with the example unit shown in Figure 2, a peak in coherence can be readily seen for the subpopulation of trackers in low frequencies of the LFP, for every modulation rate analyzed (median SFC peak frequency across modulation rates: 5.96 Hz). The subpopulation of non-tracking units, on the other hand, exhibited weaker coherence than tracking units and no visible peak in low frequencies of the spectrum, particularly in response to fast AM sounds. Additionally, higher SFC values in tracking than in non-tracking units were only clearly observed at low LFP frequencies (<12 Hz).

To address the aforementioned differences in a quantitative way, we calculated the mean coherence values in canonical low-frequency LFP bands (theta, 4–8 Hz; alpha, 8–12 Hz; low beta, 12–20 Hz; high beta, 20–30 Hz) and compared them statistically between the two neuronal groups, across modulation rates (Figure 3B). There were significant differences between the mean theta- and alpha-band SFC in response to every modulation rate tested (FDR-corrected Wilcoxon rank-sum test; corrected $p \leq 0.045$). In relatively higher frequency bands (i.e., low and high beta, 12–20 and 20–30 Hz, respectively) there were no consistent significant differences, and the z-normalized average SFC values were also not significantly different from 0 across modulation rates (FDR-corrected Wilcoxon signed rank test; corrected $p > 0.05$), with a few exceptions (for the low-beta band, at modulation rates of 5.28, 13.92, and 157.59 Hz; corrected $p < 0.012$). These results indicate that differences in coherence between tracking and non-tracking units in the AC occur in low-frequency bands (theta and alpha) of the LFP. Noteworthy, although tracking and non-tracking units also exhibited differences in their basic properties (e.g., the distribution of their best frequencies, see Figure S3), units tuned to low (<50 kHz) or high (≥50 kHz) sound frequencies did not significantly differ in their theta- or alpha-band SFC, either in the subpopulation of trackers or that of non-trackers (FDR-corrected Wilcoxon rank-sum tests, corrected $p > 0.066$ in both theta and alpha bands; data shown in Figure S4).

Considering that the definition of tracking and non-tracking units is not discrete, but to some extent graded (see previous section and Figure S1), we explored whether the strength of theta-band SFC, across modulation frequencies, would depend on the units' VS. We evaluated three conditions: one in which the considered VS of a unit was obtained in response to the specific modulation rate under consideration, a second condition in which the considered VS of a unit was obtained in response to a modulation frequency of 3.25 Hz, and a third condition in which the considered VS of a unit was calculated from responses to a modulation rate of 157.59 Hz. In these three cases, the units' SFC was grouped into four equipopulated subsets, where subset 1 contained units with the 25% lowest VS values, and subset 4, units with the 25% highest VS values. Figure S5 shows that, taking into account VS values at low modulation rates (i.e., <13.92 Hz), there was a clear relationship between the spiking synchronization strength and the SFC. Remarkably, this was true for the SFC across all modulation frequencies tested, considering VS values calculated in response to a modulation rate of 3.25 Hz (see Figure S5B), whereas no relationship was observed if the VS was computed from responses to an AM rate of 157.59 Hz (Figure S5C). The former strengthens the notion that theta-band SFC is a good marker for the coding of slow temporal envelopes in the AC.

Differences in SFC Are Not Explained by Differences in Amplitude or Phase Modulations of the LFP

We explored whether the observed differences in the SFC of trackers and non-trackers could be explained by differences in power modulations of ongoing oscillations, or by differences in LFP phase consistency across trials within a unit and modulation frequency. For that we used two approaches. First, to quantify power modulations in both groups, we calculated the phase-amplitude coupling (PAC [Tort et al., 2010]) between the LFP (same canonical bands as above) and the AM envelope across modulation frequencies. Second, to address phase consistency, we calculated the inter-trial phase coherence (ITC) of the LFP for each unit and modulation rate. Note that differences in the PAC or the ITC of tracking and non-tracking units would suggest that possible mechanisms behind the phase coding of periodic stimuli (i.e., the AM envelopes) in the AC go beyond low-frequency SFC and could also be attributed to differences in power or phase modulations of theta- or alpha-band oscillations. To be consistent, these analyses were performed on the same units used for SFC calculations (i.e., 27 trackers and 32 non-trackers).

We observed power modulations in the LFP that were related to the phase of the stimulus' envelope. The effect is shown for illustrative purposes in the high-beta band (20–30 Hz) for an example tracking unit (Figures 4A and 4B; same tracking unit shown in previous figures), in response to a modulation rate of 5.28 Hz. We chose the high-beta band to illustrate PAC effects because power modulations were typically strongest in this frequency range (see Figure 4C and [Fujioka et al., 2012]). In the example unit, the amplitude distribution of high-beta LFPs was clearly non-uniform with respect to the AM envelope's phase (Figure 4B). This non-uniformity was measured with the modulation index (MI, indicated for the example in Figure 4B), which quantifies how strongly the envelope's phase modulates the amplitude of ongoing LFPs (see Transparent Methods for details).

When comparing MIs calculated for tracking and non-tracking units at the population level, we observed no significant differences (FDR-corrected Wilcoxon rank-sum test, corrected $p > 0.09$) between the two

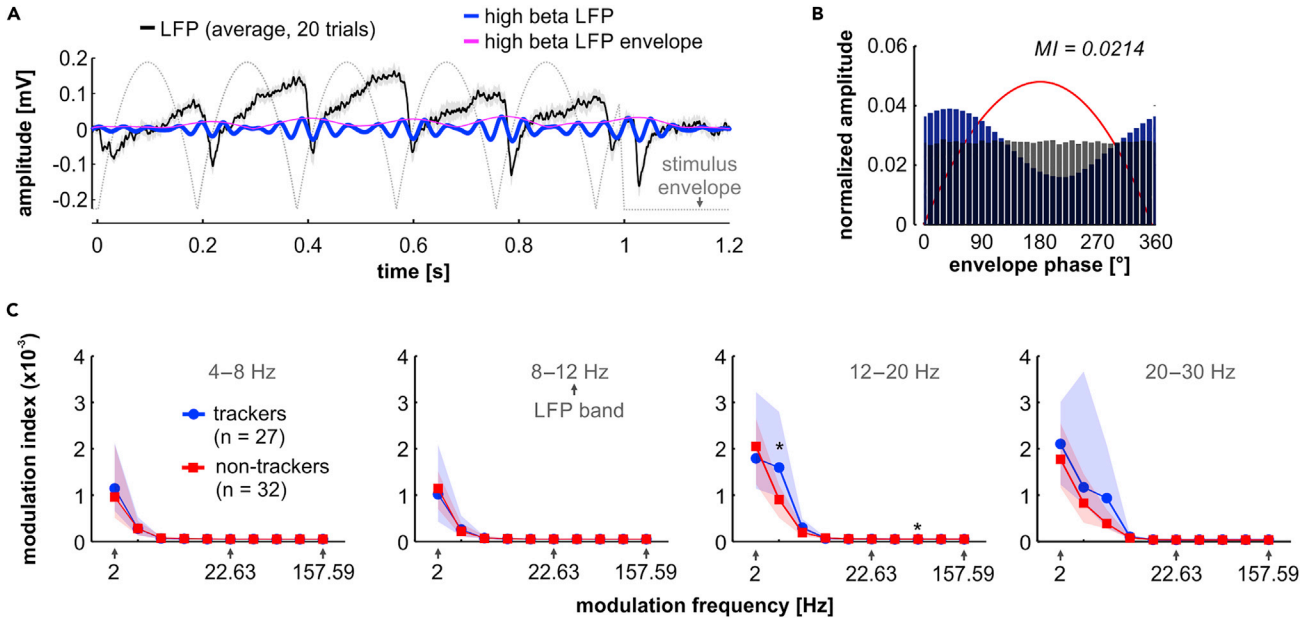

Figure 4. Phase-Amplitude Coupling in Tracking and Non-tracking Units

(A) Average LFP (black; solid line: mean; shaded area: SEM) of a tracking unit (same shown in Figure 1), in response to a modulation rate of 5.28 Hz (AM envelope shown as a dashed gray line). Average LFP filtered in high beta (20–30 Hz) is shown as a blue trace for illustrative purposes. Note the increases in amplitude at times close to the stimulus envelope's trough (the amplitude envelope of the beta-band LFP is shown in magenta).

(B) Amplitude distribution of the high-beta LFP in relation to the envelope's phase. The blue histogram shows the observed distribution of power across phases, whereas the gray histogram depicts a surrogate uniform distribution. The PAC modulation index (MI) for this unit and modulation frequency (5.28 Hz) had a value of 0.0214.

(C) Statistical comparisons (FDR-corrected Wilcoxon rank-sum tests; significance after corrected $p < 0.05$) of the PAC modulation index between tracking and non-tracking units, calculated at distinct LFP bands (indicated within the sub-panels), across modulation frequencies. There were no significant differences between the two subpopulations, except for the low-beta band (12–20 Hz), in response to modulation frequencies of 3.25 and 59.71 Hz. Units used in this analysis were the same used for SFC calculations (data is shown as median and IQR; *corrected $p < 0.05$).

groups, at nearly every LFP frequency band and AM rate tested. The latter was so, except in the case of LFPs corresponding to the low-beta band (12–20 Hz) in response to modulation frequencies of 3.25 and 59.71 Hz (corrected $p \leq 0.045$; Figure 4C). Lack of significant differences in the PAC between LFPs and AM envelopes was accompanied by lack of significant differences between the power of LFP bands of trackers and non-trackers, across modulation rates (FDR-corrected Wilcoxon rank-sum test, corrected $p > 0.06$; see Figure S6A). In addition, the modulation rate of the stimulus affected the power of the LFP bands in trackers and non-trackers (FDR-corrected Wilcoxon signed rank test; statistics summarized in Figure S6B; $p < 0.02$), in such a way that typically the power of theta, alpha, or (low and high) beta bands was higher in response to low modulation rates ($\leq$ 22.63 Hz). However, such effects do not fully explain that MI values in the PAC analyses become negligible at high modulation rates (>30 Hz; see Figure 4C). Rather, this trend is mostly due to the fact that power modulations will not occur at frequencies higher than a certain LFP band (for example, theta-band LFPs cannot carry power modulations at frequencies >8 Hz). Overall, our results indicate that differences in the SFC occurring mainly at theta and alpha bands, between tracking and non-tracking units, are not fully accounted for by differences in power modulations (or by the power itself) of the same LFP bands in both neuronal subpopulations, particularly in response to stimuli with high modulation rates (>30 Hz).

As mentioned in the preceding text, we also calculated the ITC from LFPs related to tracking and non-tracking units across modulation frequencies in the theta and alpha bands (where significant differences occurred in the SFC; Figure 5). Differences in the median ITC corresponding to trackers and non-trackers (dITC) were z-normalized to a null distribution in which the units' labels ("tracker" or "non-tracker") were randomly assigned (see Transparent Methods). The resulting z-normalized dITC between trackers and non-trackers is depicted in Figure 5 as gray traces (associated y axis on the right of the sub-panels). We observed evidence of a reset in the phase of theta- and alpha-band LFPs across modulation rates, indicated

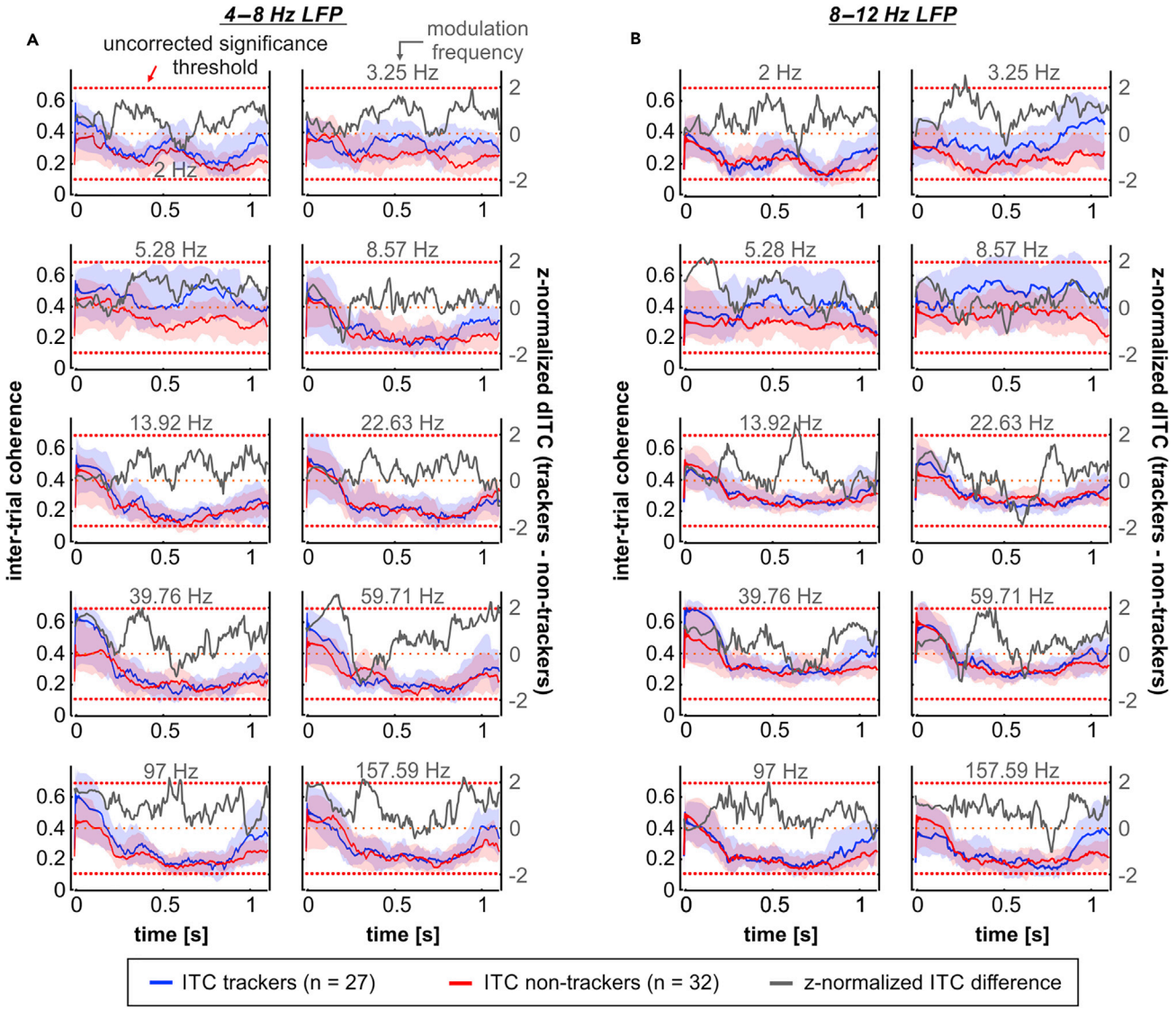

Figure 5. Inter-Trial Coherence in Tracking and Non-tracking Units

(A) Inter-trial coherence (ITC) of tracking (blue; n = 27) and non-tracking (red, n = 32; solid line, median; shaded area, interquartile range) units, across modulation frequencies (values associated to the y axis on the left), calculated with 4–8 Hz LFPs. Gray traces (associated to the y axis on the right) indicate a z-normalized (to a surrogate distribution, see Transparent Methods) difference in the median ITC of trackers and non-trackers (dITC). Horizontal red dashed lines depict an uncorrected significant threshold for the observed differences.

(B) Same as in (A), with ITC values obtained using 8–12 Hz LFPs. Units used in this analysis were the same used for SFC calculations. In every subpanel of the figure, the stimulus onset occurs at time 0.

by transiently high ITC values occurring around the stimulus onset. The former occurred considering LFPs related to either tracking or non-tracking units (Figures 5A and 5B). Moreover, ITC values in both groups were very similar (particularly in response to modulation frequencies >13.92 Hz), and the dITC between tracking and non-tracking units across modulation rates was not significantly different than what would be observed if the labels were randomly assigned. Note that the horizontal red dashed lines in Figure 5 depict an uncorrected significance threshold of z = 1.96. A z-score above 1.96 implies ITC in trackers significantly higher than in non-trackers, whereas z-scores lower than −1.96 indicate the opposite. Altogether, the results of the PAC and ITC analyses show that differences in the spike-LFP coherence at low frequencies, between tracking and non-tracking units, are not fully explained by power or phase modulations of the related LFPs in response to the stimulus.

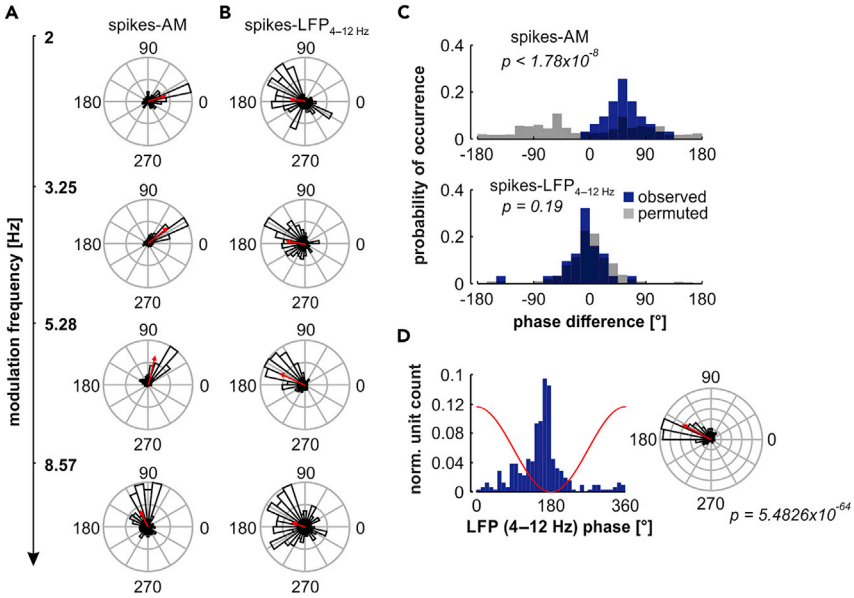

Figure 6. Spike Phases Relative to the Stimulus (but Not to Low-Frequency LFPs) Are Affected by the Envelope's Rate

(A) Spike phases obtained from an exemplary tracking unit (same shown in Figure 1) relative to the AM envelope, for modulation frequencies to which the unit's spiking was significantly synchronized (i.e., 2–8.57 Hz). Red arrows indicate the mean vector of the phase distribution.

(B) Spike phases relative to low-frequency (4–12 Hz) LFPs. Note that the spikes here are the same spikes as in (A).

(C) Top: distribution of spike-phase differences between two consecutive modulation frequencies, when phases were calculated relative to the AM envelope. The observed distribution is shown in blue, whereas a surrogate (randomized differences across not-ordered modulation frequencies) distribution is shown in gray. There was a significant difference between the randomized and observed distribution (Fisher's circular mean test, $p < 1.78 \times 10^{-8}$). Bottom: Same conventions as data shown on top, but spike phases were calculated relative to low-frequency (8–12 Hz) LFPs. No significant differences occurred between the observed and the surrogate phase difference distributions (Fisher's circular mean test, $p = 0.19$).

(D) Histogram (left) and circular histogram (right) for the distribution of preferred spike phases (relative to low-frequency LFPs) in tracking units (n = 31), across all modulation frequencies tested (i.e., all preferred phases of trackers with a cutoff frequency $\leq$ 22.63 Hz are represented). The red trace in the left histogram illustrates the phase convention relative to the LFP; the red line in the circular histogram shows the mean vector of the phase distribution. Statistics showed that there was a significant directionality in the spike phases (Rayleigh test for non-uniformity, $p = 5.48 \times 10^{-64}$).

Spike Phases Relative to Low-Frequency LFPs in Tracking Units Are Robust across Modulation Frequencies

We systematically quantified the spike-phases relative to either the stimulus envelope or to low-frequency LFPs across modulation rates. This was done with the aim of evaluating the robustness of spike timing relative to the envelope, or to low-frequency oscillations, when changes in the temporal structure of the stimulus occurred. Only trackers were included in these analyses (n = 31; cutoff frequency $\leq$ 22.63 Hz, see Figure 1), because in non-trackers significant phase relationships between the stimulus' envelope and the spikes were inexistent. Remarkably, auditory cortical units showed phase differences across modulation rates that suggested a phase lag of spikes relative to the presented stimuli as the modulation rate increased. This phase lag was evidenced by a counterclockwise rotation of the units' preferred phase in response to rising AM rates (see Figure 6A for an exemplary unit, same shown in Figure 1A). We also calculated the preferred phase of the spikes relative to low-frequency LFPs (4–12 Hz, encompassing theta and alpha bands; a separate analysis for each band is shown in Figure S7). As the modulation frequencies increased, the preferred phase of spikes to low-frequency oscillations did not change predictably across stimuli (Figure 6B).

To test for reliability in the observed spike-envelope phase lag in the subpopulation of tracking units, we calculated for each unit the differences in preferred phase between pairs of low and high modulation frequencies, organized in an increasing order. The obtained distribution was then compared with a surrogate distribution in which the order of the modulation frequencies was randomized. At the population level, the

recorded units reliably exhibited a phase lag that was represented in a clear above-zero spike-phase difference across pairs of modulation frequencies (Figure 6C, top; blue histogram). Significant differences between the observed and surrogate distributions (Figure 6C, top; gray histogram) were confirmed by a nonparametric circular median test (Fisher's circular median test, $p < 1.78 \times 10^{-8}$). In contrast, spike phases relative to low-frequency LFPs did not change predictably by increasing the modulation rate (Figure 6C, bottom; observed and surrogate differences in blue and gray, respectively), and there were no significant differences between observed and surrogate distributions (Fisher's circular median test, $p = 0.19$). The latter indicates that whereas the spikes change their stimulus-related phases (by lagging) as the envelopes' modulation rate increases, their synchronization to low-frequency oscillations is robust and independent of the stimulus modulation rate. In fact, by pooling all spike-to-LFP phases across all modulation rates, we observed that the preferred phase of spikes relative to low-frequency LFPs consistently occurred near the trough of the oscillations (Figure 6D; Rayleigh test, $p = 5.4826 \times 10^{-64}$; in the histograms, all preferred phases across tracking units and modulation frequencies are represented). This indicates a robust coupling between spikes and low-frequency cortical LFPs, and it is in line with the SFC results presented above.

Local-Field Potentials Phase Lock to AM Rates beyond the Spiking Synchronization Limits

We quantified the phase coherence between cortical oscillations and the AM stimuli, aiming to unravel whether recorded LFPs could represent amplitude envelopes to which the spiking activity did not synchronize. Coherence between LFPs and stimulus envelope, per modulation rate, was calculated using the stimulus-field coherence (StimFC) metric. The StimFC is a normalized, frequency-dependent synchronization index, which measures the strength of coherence between ongoing oscillatory activity and the auditory stimulus. The StimFC and SFC analyses are conceptually similar, but to evaluate phase locking between the AM envelopes and cortical oscillations, LFP windows were always defined in the range starting at 100 ms after stimulus onset and ending at the stimulus offset (i.e., windows were 900 ms long). Note that to obtain StimFC values, unit specificity was sacrificed to increase the robustness of coherence estimates. Thus, 300 LFP segments were chosen randomly, per modulation frequency, from a pool that included all trials from all units, depending on their classification as trackers or non-trackers. To reduce sampling biases, the procedure was repeated 500 times (see Transparent Methods for details).

The stimulus-triggered averages (i.e., the mean of the LFP segments; StimTAs) revealed that, independently of the modulation frequency analyzed, oscillations in the AC were synchronized to the envelope's periodicity. Remarkably, we observed that even the highest modulation rate tested (157.59 Hz) entrained cortical field potentials, as depicted in Figure 7A. Note that the inset in the panel shows clear oscillatory activity in the LFP average, which matches the envelope's repetition rate. This entrainment did not occur when the phase consistency across trials was reduced to chance (red traces in the figure). Consequently, the spectra of the StimTAs clearly peaked at frequencies related to the modulation rate of the stimulus, which was not the case for the spectra of surrogate LFP averages (Figure 7B; black, observed; red, surrogate). Figure 7C shows the average spectrum of individual LFP windows used to obtain stimulus-triggered averages (also referred to as stimulus-triggered power, or StimTP). Spectral peaks were clearly present around frequencies related to the stimulus envelope in both observed and surrogate data (black and red traces in Figure 7C, respectively), which indicates that whereas the phase consistency was greatly reduced across trials for surrogate LFP windows, the power of individual segments was not equally affected. The StimFC (Figure 7D) was obtained after normalizing the power of the StimTA with the StimTP, and coherence values obtained from intact data were z-normalized to the distribution of coherence values obtained from surrogate data (z-normalized StimFC, shown in the inset of Figure 7D). Figure 7E depicts z-normalized StimFC values across modulation frequencies, for the population of trackers (blue) and non-trackers (red). Independently of the neuronal subgroup considered, LFPs in the AC were able to synchronize to AM envelopes with rates of at least 157.59 Hz, evidenced by the coherence peaks at frequencies related to the modulation rate under consideration, and at harmonics of such frequencies. The appearance of harmonics could be partly explained by nonlinearities in the processing of AM sounds along the auditory pathway (John and Picton, 2000; Prendergast et al., 2010).

DISCUSSION

In this study, we investigated how LFPs interact with spikes for the representation of amplitude-modulated sounds. In a previous article we had already shown that, similar to other mammals, in the bat *C. perspicillata* the majority of cortical units cannot represent the temporal structure of fast (>22.63 Hz) AM sounds with a phase code (Martin et al., 2017). Here, using *C. perspicillata* as an animal model, we present three major

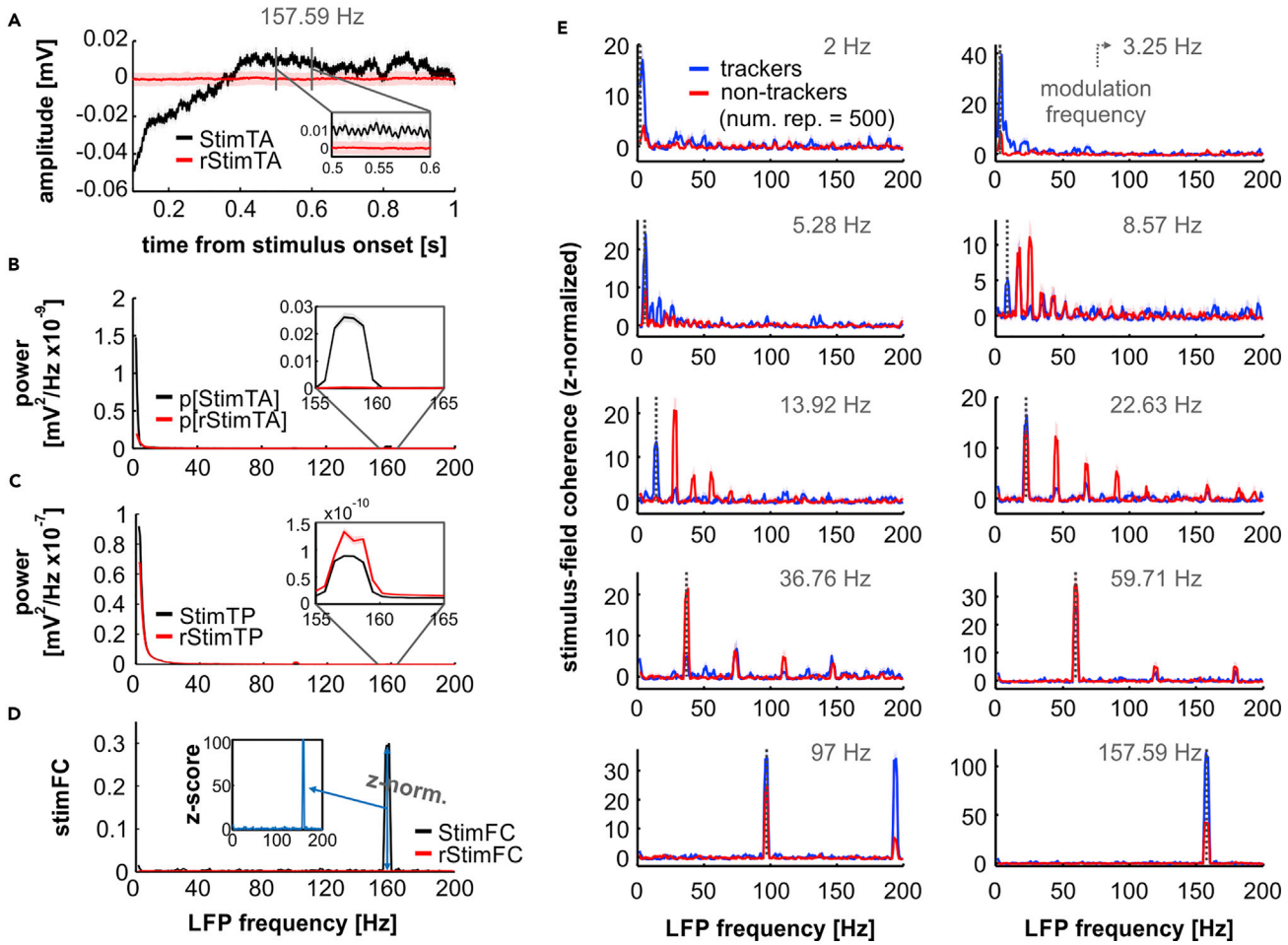

Figure 7. Local-Field Potentials Phase Lock to High-Frequency AM Envelopes

(A) Stimulus-triggered average (StimTA; black traces) related to tracking units, in response to a modulation frequency of 157.59 Hz (StimTAs over 500 repetitions). The StimTA preserves LFP components that are phase coherent to the stimulus (see Transparent Methods) and is obtained by averaging LFP windows (n = 300, randomly chosen a total of m = 500 times) associated to a particular time point (here, the 100-ms mark after stimulus onset). Randomized StimTAs are shown in red traces.

(B) Power of the StimTAs shown in A (black traces). Note that the StimTA spectrum peaks at frequencies related to the modulation rate of the stimulus, whereas the spectrum of surrogate StimTAs does not.

(C) Stimulus-triggered power (StimTP) of the LFP segments used to calculate StimTAs in (A). There is power in the LFP at frequencies around the modulation rate of the presented sounds, also when considering surrogate LFP segments (red trace).

(D) Stimulus-field coherence (StimFC; black) of recorded LFPs in response to a modulation frequency of 157.69 Hz. Calculated StimFC values were z-normalized to a baseline StimFC and are shown in the inset (light blue trace).

(E) z-normalized StimFC values across modulation rates (indicated in each sub-panel) for the subpopulations of tracking (blue) and non-tracking (red) units. Data in the figure are shown as median (solid lines) and quartiles (shaded areas).

findings that shed light onto the dynamics of temporal processing in the AC from an oscillatory coherence perspective. (1) SFC is stronger in units that elicit stimulus phase-locked responses (trackers) than in those that do not (non-trackers), even at modulation rates beyond their synchronization abilities. (2) AM envelopes modulate the amplitude and phase of low-frequency LFPs, but these modulations do not reliably account for differences in coherence between tracking and non-tracking units. (3) Spike phases relative to low-frequency LFPs (4–12 Hz) were robust across modulation rates, whereas spike phases relative to the stimuli were not. The implications of these findings are discussed below.

Neuronal Responses in the AC Exhibit Limited Tracking Capacities

The majority of recorded units had cutoff frequencies less than or equal to 22.63 Hz. Interestingly, we observed that cortical tracking units do not always synchronize to the same phase of the sound envelope

across modulation rates; rather, spike phases relative to the envelope showed an increasing lag in response to faster envelopes (see Figures 6 and S1B). Similar phase differences have been observed in subcortical structures (Krishna and Semple, 2000), although not in the AC. The phase-locking threshold reported for auditory cortical units of *C. perspicillata* is consistent with results from previous studies showing that, in a variety of animal species, synchronized cortical responses have limiting modulation frequencies of around 25–35 Hz (Creutzfeldt et al., 1980; Schreiner and Urbas, 1988; Gaese and Ostwald, 1995; Fitzpatrick et al., 2009). Vocalizations of the bat species used in this study can carry AMs higher than 60 Hz (Hechavarria et al., 2016), and despite the reported phase-locking limitations such fast temporal structures can still be encoded in the bat's AC. The AC does not solely rely on a phase code to represent fast AM envelopes: rate coding is also a possible mechanism, whereby neurons alter their firing according to the stimulus' periodicity (Lu et al., 2001; Bendor and Wang, 2007; Gao et al., 2016; Tang et al., 2016). In a recent article, we reported that rate-coding neurons exist in the AC of *C. perspicillata* (Martin et al., 2017), which was corroborated in our present data (see Figure S2). Another possible way of representing fast envelopes in the AC is by means of fast trackers. Our data show that a small set of units phase-lock their spikes to envelopes above 30 Hz (see cutoff distribution in Figure 1F). These units were not considered in the analyses because their occurrence was rare (11.49% of the total recorded units), and our main interest lied in unraveling possible mechanisms underlying periodicity coding in the mammalian AC, by means of low-frequency LFPs. Nevertheless, note that neurons synchronized to modulation rates >30 Hz have also been reported in the AC of awake primates (Bieser and Muller-Preuss, 1996).

Local-Field Potentials in the Auditory Cortex Synchronize to Fast AM Rates

In contrast to the limited phase-locking abilities of the cortical spiking, LFPs were well synchronized to AM envelopes with modulation frequencies of at least 157.59 Hz (see Figure 7). The entrainment of high-frequency LFPs to fast temporal structures in the AC of *C. perspicillata* has also been reported in a previous study, in which cortical field potentials were shown to follow the syllabic rate of conspecific distress vocalizations, at frequencies >60 Hz (Hechavarria et al., 2016). However, phase synchronization of cortical oscillations to rates of at least 40 Hz is not an exclusive property of *C. perspicillata*'s cortex, as oscillatory entrainment to fast-varying stimuli has also been reported in rats (Li et al., 2018; Wang et al., 2018). In humans, several electroencephalography and magnetoencephalography studies have shown auditory steady-state responses to AM envelopes with modulation frequencies as high as 80 Hz (Lins et al., 1995; John and Picton, 2000; Prendergast et al., 2010). In fact, the entrainment of gamma-band oscillations to fast-varying (>40 Hz) temporal structures in the AC is well documented as a mechanism for the cortical processing of the phonemic rate present in speech signals (Giraud and Poeppel, 2012).

It would be highly speculative to attribute the cause of high-frequency stimulus-coherent LFPs to a specific phenomenon along the auditory pathway. With our data, we cannot disentangle whether the observed oscillations are the result of potentials propagating passively in the conductive volume, or whether these cortical LFPs originate from synaptic inputs to the AC. Both possibilities are indeed feasible. In the AC of awake primates, subthreshold membrane potentials synchronize to AM sounds modulated at frequencies >30 Hz, which the spiking activity can no longer track in a phasic manner (Gao et al., 2016). Considering the fact that LFPs are affected by the membrane potentials (Buzsaki et al., 2012), it is possible that high-frequency LFP synchronization could be in part a consequence of synaptic potentials reflecting thalamic inputs (as the thalamus follows repetition rates of >100 Hz [Creutzfeldt et al., 1980; Rouiller et al., 1981]). On the other hand, previous studies in humans have shown that the sources of oscillatory responses to AM sounds depend on the modulation frequencies being heard: low frequencies are generated by cortical sources, whereas high frequencies (>40 Hz) are typically preferred by subcortical levels (Herdman et al., 2002; Farahani et al., 2017). Considering that neurons in subcortical auditory structures (e.g., the thalamus or the inferior colliculus) are able to phase lock to AM envelopes with frequencies >100 Hz (Joris et al., 2004), it is conceivable that potentials related to evoked activity in these structures propagate and reach the AC. However, we point out that these two phenomena (phase-locked subthreshold membrane potentials and passive propagation from lower order structures) are not mutually exclusive, and contributions from both might shape the dynamics of LFP coherence to fast varying acoustic streams.

Our data reveal LFP entrainment to AM rates of 36.76 and 59.71 Hz, two frequencies that fall within the canonical low-gamma range, spanning from 30 to 60 Hz. We note that it would be inaccurate to claim that these fluctuations in the gamma range subserve computational operations analogous to those typically described in the visual system, such as feature binding or neuronal communication (Fries et al., 2001;

Womelsdorf et al., 2007; Fries, 2009, 2015; Singer, 2017). Rather, the oscillatory activity at those frequencies, in our data, represents a phase alignment strongly driven by the temporal structure of the AM envelope. Nevertheless, this does not imply that gamma oscillations do not participate in the encoding of sounds in the AC. An increase of gamma-band activity, linked to the processing of auditory stimuli, has been reported in humans (Pantev et al., 1991), non-human primates (Brosch et al., 2002), rats (Vianney-Rodrigues et al., 2011), and bats (Medvedev and Kanwal, 2008). Gamma-band oscillations in these studies (except for the one conducted on human subjects) were also correlated to some extent with neuronal spiking, something that we did not observe in our data (see Figures 2 and 3). We speculate the following main reasons for this disparity: (1) gamma oscillations, if temporally aligned to listened sounds, occurred in the early portion of short auditory stimuli, whereas our analyses were conducted in the range of 100 ms to 1s after stimulus onset; (2) induced gamma activity (i.e., not phase locked to specific portions of the stimulus) would have been masked by phase coherence analyses such as the SFC or StimFC; and (3) gamma-band LFPs might not be crucial for phase coding of slow temporal envelopes in the AC. In line with the last statement, tracking and non-tracking responses may instead be mediated by low-frequency oscillations, in the theta-alpha range. The possible contributions of low-frequency oscillations to periodicity coding in the cortex are addressed in the following section.

Roles of Low-Frequency Spike-LFP Coherence for Phase Coding in the AC

We showed that units in the AC capable to lock their spiking to the periodic temporal structure of AM envelopes (that is, trackers) synchronize more strongly to low-frequency LFPs than their non-tracking counterparts. In other words, the SFC of cortical tracking units in the theta-alpha range is higher than that in non-tracking units. Importantly, differences in low-frequency coherence between cortical trackers and non-trackers occurred well beyond the synchronization limits of neurons in the AC to AM sounds (up to modulation rates of 157.59 Hz; see Figures 1, 2, and 3). Moreover, neither PAC between the stimulus phase and the amplitude of low-frequency LFPs (Figure 4) nor the ITC of the units' LFPs across modulation rates (Figure 5) allowed to reliably separate trackers from non-trackers. A reliable classification (in terms of low-frequency LFP bands) was only possible when considering the SFC, mostly at theta (4–8 Hz) and alpha (8–12 Hz) bands. The former, together with the fact that spikes and slow oscillations maintain a robust phase relationship across modulation rates (see Figure 6), suggests that low-frequency waves might be important for periodicity coding.

The origins of theta and alpha oscillations in the AC remain somewhat unexplored. Evidence from *in vivo* experiments in the visual cortex suggests that oscillatory processes in the range of 5–10 Hz are generated by pacemaking pyramidal neurons located in infragranular layers of the cortical column, whose membrane temporal dynamics correspond with the aforementioned rhythms (Sun and Dan, 2009). In the auditory modality, Szymanski and colleagues observed that fast activations in the thalamo-recipient layers in the AC produce strong phase resets in ongoing low-frequency LFPs, which could explain, in part, their entrainment to sensory input (Szymanski et al., 2011). Although the resulting phase alignment in such scenario would be dependent on thalamic inputs (and therefore could be considered as evoked), there is strong evidence suggesting that cortical oscillatory activity also represents modulatory (as opposed to evoked) influences. For example, in the macaque brain, somatosensory inputs modulate the phase of delta- and theta-band oscillations in primary AC, which results in enhanced processing of acoustic stimuli (Lakatos et al., 2007). Importantly, these phase modulations occur not only during multimodal sensory processing but also as a consequence of attentional mechanisms, which could be regulated by higher order structures (Schroeder and Lakatos, 2009; Arnal and Giraud, 2012; Lakatos et al., 2013).

In the AC, low-frequency field potentials regulate the amplitude of faster oscillations, together with the neuronal excitability, in a hierarchical manner (Lakatos et al., 2005). These low-frequency oscillations can reliably entrain to periodic acoustic streams, whether the periodicity is present in the temporal (Lakatos et al., 2005, 2013; Luo et al., 2010; Arnal and Giraud, 2012; Giraud and Poeppel, 2012) or the spectral (Henry and Obleser, 2012) structure of the stimulus. For example, the phase patterns of theta oscillations are stable (and unique) enough to discriminate speech on a single trial basis (Luo and Poeppel, 2007). This implies that the phase of delta and theta bands might actively modulate the cortical spiking and the power of higher frequency LFPs according to the sensory input, such that a multiplexed cortical activity would enhance the representation of acoustic stimuli (Gross et al., 2013; Hyafil et al., 2015). Furthermore, there is strong evidence supporting the roles of entrained low-frequency oscillations in modulating behavioral performance during detection tasks (Ng et al., 2012; Lawrance et al., 2014). When there is entrainment

of low-frequency oscillations (see Henry and Obleser, 2012; Lawrance et al., 2014), enhanced detection could be explained by the predictive coding framework. From the point of view of predictive coding, entrainment could allow sensory predictions (represented by the phase of low-frequency oscillations) to temporally align with relevant stimuli, and thus enhance their representation in the brain (Arnal and Giraud, 2012). Overall, the above indicates that low-frequency oscillations in the auditory domain play an important role for coordinating efficient neuronal responses to acoustic (and predictive) stimuli.

Our results resonate with the aforementioned views, showing that spike coherence to low-frequency LFPs is (at least) a fingerprint of periodicity coding in the AC. Based on our observations, we speculate that neurons whose spiking patterns are coupled to slow cortical oscillations profit from the phase relationship of these low-frequency waves with the periodicity of acoustic streams. On the contrary, neurons not phase synchronized to low-frequency LFPs do not profit from the aforementioned LFP-stimulus phase relationship, and do not elicit temporally organized spikes that track the rhythms of the AM envelopes. Altogether, our data suggest that low-frequency SFC could play an important role in orchestrating the phasic representation of rhythmic stimuli in the AC.

METHODS

All methods can be found in the accompanying Transparent Methods supplemental file.

SUPPLEMENTAL INFORMATION

Supplemental Information includes Transparent Methods and seven figures and can be found with this article online at https://doi.org/10.1016/j.isci.2018.10.009.

ACKNOWLEDGMENTS

The German Research Council (DFG) funded this work (Grant No. HE 7478/1-1).

AUTHOR CONTRIBUTIONS

F.G.R. and J.C.H. designed the study. F.G.R. collected the data. F.G.R. analyzed the data and wrote the manuscript. F.G.R., L.M.M., M.J.B., Y.C.C., M.K., and J.C.H. discussed the results and reviewed the manuscript.

DECLARATION OF INTERESTS

The authors declare no competing interests.

Received: December 5, 2017
Revised: June 20, 2018
Accepted: October 10, 2018
Published: November 30, 2018

REFERENCES

Arnal, L.H., Flinker, A., Kleinschmidt, A., Giraud, A.L., and Poeppel, D. (2015). Human screams occupy a privileged niche in the communication soundscape. Curr. Biol. *25*, 2051–2056.

Arnal, L.H., and Giraud, A.L. (2012). Cortical oscillations and sensory predictions. Trends Cogn. Sci. *16*, 390–398.

Bendor, D., and Wang, X. (2007). Differential neural coding of acoustic flutter within primate auditory cortex. Nat. Neurosci. *10*, 763–771.

Bieser, A., and Muller-Preuss, P. (1996). Auditory responsive cortex in the squirrel monkey: neural responses to amplitude-modulated sounds. Exp. Brain Res. *108*, 273–284.

Brosch, M., Budinger, E., and Scheich, H. (2002). Stimulus-related gamma oscillations in primate auditory cortex. J. Neurophysiol. *87*, 2715–2725.

Buzsaki, G., Anastassiou, C.A., and Koch, C. (2012). The origin of extracellular fields and currents–EEG, ECoG, LFP and spikes. Nat. Rev. Neurosci. *13*, 407–420.

Creutzfeldt, O., Hellweg, F.C., and Schreiner, C. (1980). Thalamocortical transformation of responses to complex auditory stimuli. Exp. Brain Res. *39*, 87–104.

Drullman, R., Festen, J.M., and Plomp, R. (1994). Effect of reducing slow temporal modulations on speech reception. J. Acoust. Soc. Am. *95*, 2670–2680.

Farahani, E.D., Goossens, T., Wouters, J., and van Wieringen, A. (2017). Spatiotemporal reconstruction of auditory steady-state responses to acoustic amplitude modulations: potential sources beyond the auditory pathway. Neuroimage *148*, 240–253.

Fitzpatrick, D.C., Roberts, J.M., Kuwada, S., Kim, D.O., and Filipovic, B. (2009). Processing temporal modulations in binaural and monaural auditory stimuli by neurons in the inferior colliculus and auditory cortex. J. Assoc. Res. Otolaryngol. *10*, 579–593.

Fries, P. (2009). Neuronal gamma-band synchronization as a fundamental process in cortical computation. Annu. Rev. Neurosci. *32*, 209–224.

Fries, P. (2015). Rhythms for cognition: communication through coherence. Neuron *88*, 220–235.

Fries, P., Neuenschwander, S., Engel, A.K., Goebel, R., and Singer, W. (2001). Rapid feature selective neuronal synchronization through correlated latency shifting. Nat. Neurosci. *4*, 194–200.

Fujioka, T., Trainor, L.J., Large, E.W., and Ross, B. (2012). Internalized timing of isochronous sounds is represented in neuromagnetic beta oscillations. J. Neurosci. *32*, 1791–1802.

Gaese, B.H., and Ostwald, J. (1995). Temporal coding of amplitude and frequency modulation in the rat auditory cortex. Eur. J. Neurosci. *7*, 438–450.

Gao, L., Kostlan, K., Wang, Y., and Wang, X. (2016). Distinct subthreshold mechanisms underlying rate-coding principles in primate auditory cortex. Neuron *91*, 905–919.

Giraud, A.L., and Poeppel, D. (2012). Cortical oscillations and speech processing: emerging computational principles and operations. Nat. Neurosci. *15*, 511–517.

Grasse, D.W., and Moxon, K.A. (2010). Correcting the bias of spike field coherence estimators due to a finite number of spikes. J. Neurophysiol. *104*, 548–558.

Gross, J., Hoogenboom, N., Thut, G., Schyns, P., Panzeri, S., Belin, P., and Garrod, S. (2013). Speech rhythms and multiplexed oscillatory sensory coding in the human brain. PLoS Biol. *11*, e1001752.

Hechavarria, J.C., Beetz, M.J., Macias, S., and Kossl, M. (2016). Vocal sequences suppress spiking in the bat auditory cortex while evoking concomitant steady-state local field potentials. Sci. Rep. *6*, 39226.

Henry, M.J., and Obleser, J. (2012). Frequency modulation entrains slow neural oscillations and optimizes human listening behavior. Proc. Natl. Acad. Sci. U S A *109*, 20095–20100.

Herdman, A.T., Lins, O., Van Roon, P., Stapells, D.R., Scherg, M., and Picton, T.W. (2002). Intracerebral sources of human auditory steady-state responses. Brain Topogr. *15*, 69–86.

Hyafil, A., Fontolan, L., Kabdebon, C., Gutkin, B., and Giraud, A.L. (2015). Speech encoding by coupled cortical theta and gamma oscillations. Elife *4*, e06213.

John, M.S., and Picton, T.W. (2000). Human auditory steady-state responses to amplitude-modulated tones: phase and latency measurements. Hear. Res. *141*, 57–79.

Johnson, J.S., Yin, P., O'Connor, K.N., and Sutter, M.L. (2012). Ability of primary auditory cortical neurons to detect amplitude modulation with rate and temporal codes: neurometric analysis. J. Neurophysiol. *107*, 3325–3341.

Joris, P.X., Schreiner, C.E., and Rees, A. (2004). Neural processing of amplitude-modulated sounds. Physiol. Rev. *84*, 541–577.

Kanwal, J.S., Matsumura, S., Ohlemiller, K., and Suga, N. (1994). Analysis of acoustic elements and syntax in communication sounds emitted by mustached bats. J. Acoust. Soc. Am. *96*, 1229–1254.

Kayser, C., Montemurro, M.A., Logothetis, N.K., and Panzeri, S. (2009). Spike-phase coding boosts and stabilizes information carried by spatial and temporal spike patterns. Neuron *61*, 597–608.

Koch, U., and Grothe, B. (2000). Interdependence of spatial and temporal coding in the auditory midbrain. J. Neurophysiol. *83*, 2300–2314.

Krishna, B.S., and Semple, M.N. (2000). Auditory temporal processing: responses to sinusoidally amplitude-modulated tones in the inferior colliculus. J. Neurophysiol. *84*, 255–273.

Lakatos, P., Chen, C.M., O'Connell, M.N., Mills, A., and Schroeder, C.E. (2007). Neuronal oscillations and multisensory interaction in primary auditory cortex. Neuron *53*, 279–292.

Lakatos, P., Musacchia, G., O'Connel, M.N., Falchier, A.Y., Javitt, D.C., and Schroeder, C.E. (2013). The spectrotemporal filter mechanism of auditory selective attention. Neuron *77*, 750–761.

Lakatos, P., Shah, A.S., Knuth, K.H., Ulbert, I., Karmos, G., and Schroeder, C.E. (2005). An oscillatory hierarchy controlling neuronal excitability and stimulus processing in the auditory cortex. J. Neurophysiol. *94*, 1904–1911.

Lawrance, E.L., Harper, N.S., Cooke, J.E., and Schnupp, J.W. (2014). Temporal predictability enhances auditory detection. J. Acoust. Soc. Am. *135*, EL357–EL363.

Li, S., Ma, L., Wang, Y., Wang, X., Li, Y., and Qin, L. (2018). Auditory steady-state responses in primary and non-primary regions of the auditory cortex in neonatal ventral hippocampal lesion rats. PLoS One *13*, e0192103.

Lins, O.G., Picton, P.E., Picton, T.W., Champagne, S.C., and Durieux-Smith, A. (1995). Auditory steady-state responses to tones amplitude-modulated at 80-110 Hz. J. Acoust. Soc. Am. *97*, 3051–3063.

Lu, T., Liang, L., and Wang, X. (2001). Temporal and rate representations of time-varying signals in the auditory cortex of awake primates. Nat. Neurosci. *4*, 1131–1138.

Lu, T., and Wang, X. (2000). Temporal discharge patterns evoked by rapid sequences of wide- and narrowband clicks in the primary auditory cortex of cat. J. Neurophysiol. *84*, 236–246.

Luo, H., Liu, Z., and Poeppel, D. (2010). Auditory cortex tracks both auditory and visual stimulus dynamics using low-frequency neuronal phase modulation. PLoS Biol. *8*, e1000445.

Luo, H., and Poeppel, D. (2007). Phase patterns of neuronal responses reliably discriminate speech in human auditory cortex. Neuron *54*, 1001–1010.

Luo, H., Wang, Y., Poeppel, D., and Simon, J.Z. (2007). Concurrent encoding of frequency and amplitude modulation in human auditory cortex: encoding transition. J. Neurophysiol. *98*, 3473–3485.

Malone, B.J., Scott, B.H., and Semple, M.N. (2007). Dynamic amplitude coding in the auditory cortex of awake rhesus macaques. J. Neurophysiol. *98*, 1451–1474.

Martin, L.M., Garcia-Rosales, F., Beetz, M.J., and Hechavarria, J.C. (2017). Processing of temporally patterned sounds in the auditory cortex of Seba's short-tailed bat, *Carollia perspicillata*. Eur. J. Neurosci. *46*, 2365–2379.

Medvedev, A.V., and Kanwal, J.S. (2008). Communication call-evoked gamma-band activity in the auditory cortex of awake bats is modified by complex acoustic features. Brain Res. *1188*, 76–86.

Middlebrooks, J.C. (2015). Sound localization. Handb. Clin. Neurol. *129*, 99–116.

Ng, B.S.W., Schroeder, T., and Kayser, C. (2012). A precluding but not ensuring role of entrained low-frequency oscillations for auditory perception. J. Neurosci. *32*, 12268–12276.

Niwa, M., O'Connor, K.N., Engall, E., Johnson, J.S., and Sutter, M.L. (2015). Hierarchical effects of task engagement on amplitude modulation encoding in auditory cortex. J. Neurophysiol. *113*, 307–327.

Palva, S., and Palva, J.M. (2011). Functional roles of alpha-band phase synchronization in local and large-scale cortical networks. Front. Psychol. *2*, 204.

Pantev, C., Makeig, S., Hoke, M., Galambos, R., Hampson, S., and Gallen, C. (1991). Human auditory evoked gamma-band magnetic fields. Proc. Natl. Acad. Sci. U S A *88*, 8996–9000.

Prendergast, G., Johnson, S.R., and Green, G.G. (2010). Temporal dynamics of sinusoidal and non-sinusoidal amplitude modulation. Eur. J. Neurosci. *32*, 1599–1607.

Rhode, W.S., and Greenberg, S. (1994). Encoding of amplitude modulation in the cochlear nucleus of the cat. J. Neurophysiol. *71*, 1797–1825.

Rouiller, E., de Ribaupierre, Y., Toros-Morel, A., and de Ribaupierre, F. (1981). Neural coding of repetitive clicks in the medial geniculate body of cat. Hear. Res. *5*, 81–100.

Schreiner, C.E., and Urbas, J.V. (1988). Representation of amplitude modulation in the auditory cortex of the cat. II. Comparison between cortical fields. Hear. Res. *32*, 49–63.

Schroeder, C.E., and Lakatos, P. (2009). Low-frequency neuronal oscillations as instruments of sensory selection. Trends Neurosci. *32*, 9–18.

Shannon, R.V., Zeng, F.G., Kamath, V., Wygonski, J., and Ekelid, M. (1995). Speech recognition with primarily temporal cues. Science *270*, 303–304.

Singer, W. (2018). Neuronal oscillations: unavoidable and useful? Eur. J. Neurosci. 1–10.

Slama, M.C., and Delgutte, B. (2015). Neural coding of sound envelope in reverberant environments. J. Neurosci. *35*, 4452–4468.

Stefanics, G., Hangya, B., Hernadi, I., Winkler, I., Lakatos, P., and Ulbert, I. (2010). Phase entrainment of human delta oscillations can mediate the effects of expectation on reaction speed. J. Neurosci. *30*, 13578–13585.

Suga, N. (2015). Neural processing of auditory signals in the time domain: delay-tuned coincidence detectors in the mustached bat. Hear. Res. *324*, 19–36.

Sun, W., and Dan, Y. (2009). Layer-specific network oscillation and spatiotemporal receptive field in the visual cortex. Proc. Natl. Acad. Sci. U S A *106*, 17986–17991.

Szymanski, F.D., Rabinowitz, N.C., Magri, C., Panzeri, S., and Schnupp, J.W. (2011). The laminar and temporal structure of stimulus information in the phase of field potentials of auditory cortex. J. Neurosci. *31*, 15787–15801.

Tang, H.Z., Crain, S., and Johnson, B.W. (2016). Dual temporal encoding mechanisms in human auditory cortex: evidence from MEG and EEG. Neuroimage *128*, 32–43.

Theunissen, F.E., and Doupe, A.J. (1998). Temporal and spectral sensitivity of complex auditory neurons in the nucleus HVc of male zebra finches. J. Neurosci. *18*, 3786–3802.

Tort, A.B., Komorowski, R., Eichenbaum, H., and Kopell, N. (2010). Measuring phase-amplitude coupling between neuronal oscillations of different frequencies. J. Neurophysiol. *104*, 1195–1210.

Vianney-Rodrigues, P., Iancu, O.D., and Welsh, J.P. (2011). Gamma oscillations in the auditory cortex of awake rats. Eur. J. Neurosci. *33*, 119–129.

Wang, Y., Ma, L., Wang, X., and Qin, L. (2018). Differential modulation of the auditory steady state response and inhibitory gating by chloral hydrate anesthesia. Sci. Rep. *8*, 3683.

Wohlgemuth, M.J., Luo, J., and Moss, C.F. (2016). Three-dimensional auditory localization in the echolocating bat. Curr. Opin. Neurobiol. *41*, 78–86.

Womelsdorf, T., and Fries, P. (2007). The role of neuronal synchronization in selective attention. Curr. Opin. Neurobiol. *17*, 154–160.

Womelsdorf, T., Schoffelen, J.M., Oostenveld, R., Singer, W., Desimone, R., Engel, A.K., and Fries, P. (2007). Modulation of neuronal interactions through neuronal synchronization. Science *316*, 1609–1612.

Yin, P.B., Johnson, J.S., O'Connor, K.N., and Sutter, M.L. (2011). Coding of amplitude modulation in primary auditory cortex. J. Neurophysiol. *105*, 582–600.

ISCI, Volume *9*

Supplemental Information

Low-Frequency Spike-Field Coherence Is a Fingerprint of Periodicity Coding in the Auditory Cortex

Francisco García-Rosales, Lisa M. Martin, M. Jerome Beetz, Yuranny Cabral-Calderin, Manfred Kössl, and Julio C. Hechavarria

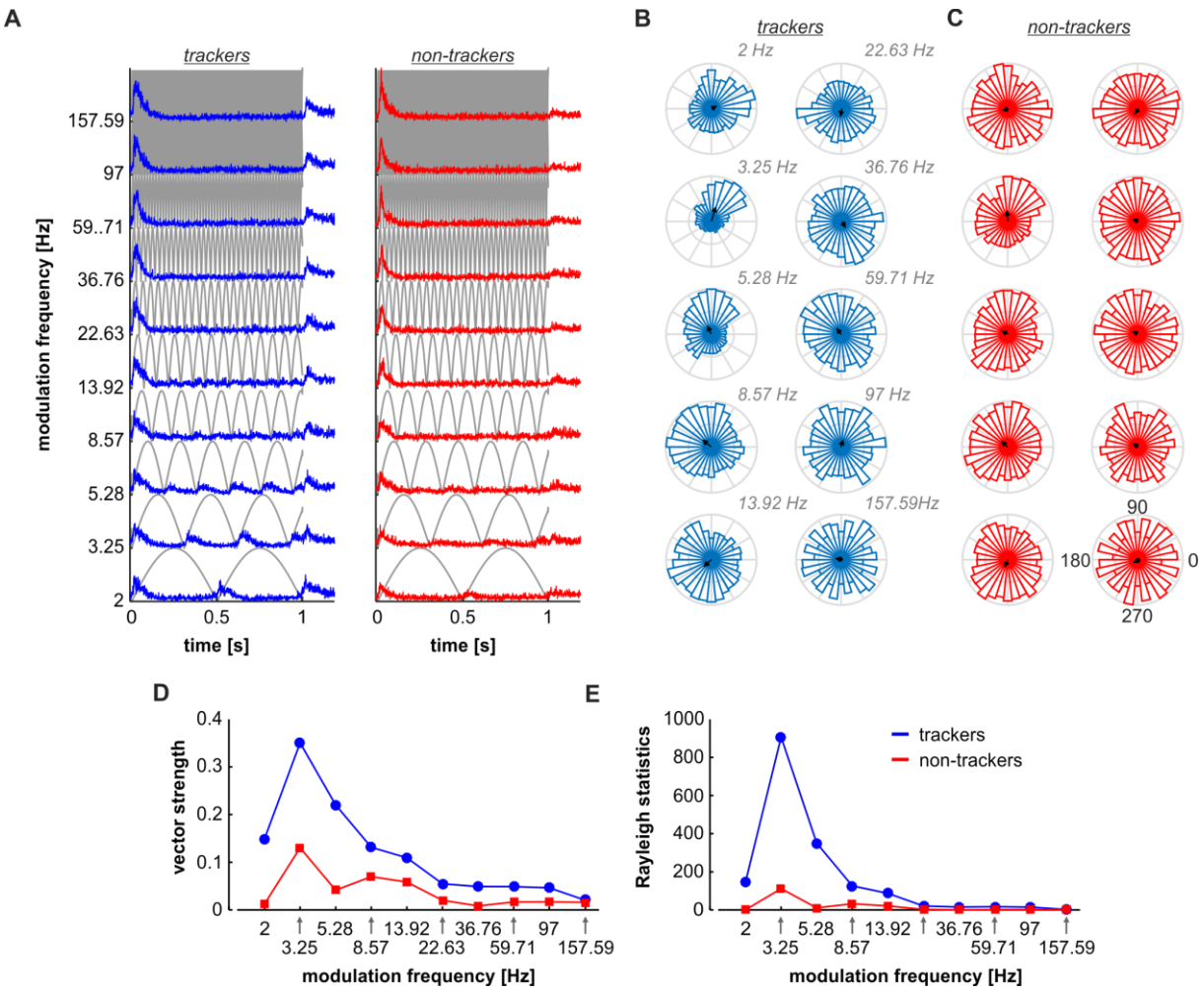

Fig. S1. Pooled responses reveal weak temporal organization for non-tracking units (related to Figure 1). (**A**) Normalized peri-stimulus time histograms (PSTH) calculated from the pooled activity of tracking (blue, left) and non-tracking (red, right) units, in response to all modulation frequencies tested. (**B**) Distribution of spike-phases relative to the AM envelopes, across modulation frequencies, for the pooled spiking of tracking units. Circular histograms show that spike-phases are well-grouped up to modulation rates of 22.63 Hz, suggesting that units fire at similar phases in response to the same modulation frequency. Black arrows represent the mean vector for the phase distribution. (**C**) Spike-phases relative to the AM envelope, across modulation rates, for the pooled spiking of non-tracking units. A weak but still visible clustering of the spike-phases occurs in response to modulation frequencies < 22.63 Hz, particularly at AM rates of 3.25 and 8.57 Hz. (**D**) Vector strength (VS) calculated for the pooled spiking of tracking (blue) and non-tracking (red) units. (**E**) Rayleigh statistics of the spike-phases for pooled tracking (blue) and non-tracking (red) units.

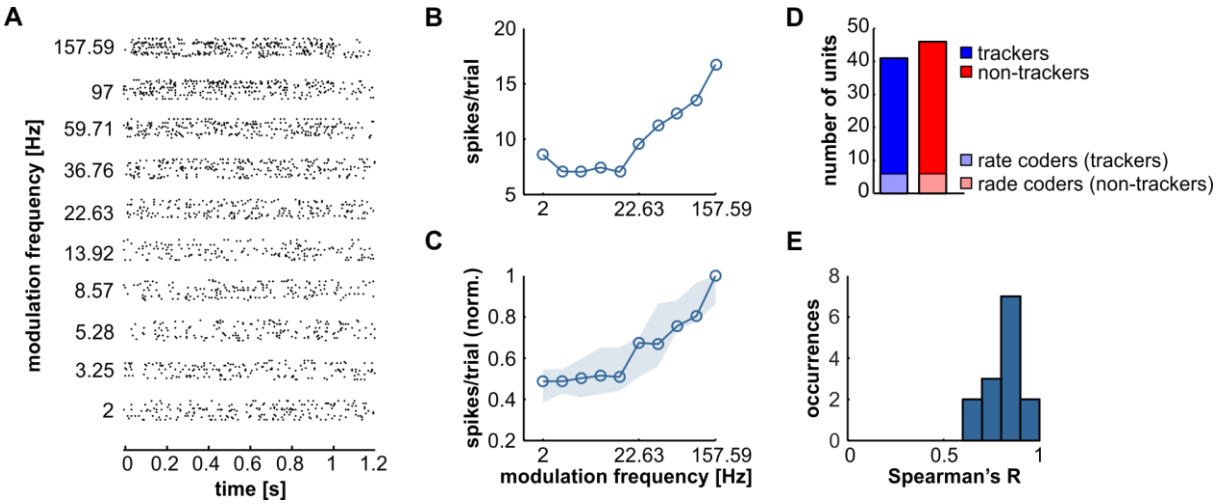

Fig. S2. Rate coding in the auditory cortex of *Carollia perspicillata* (related to Figure 1). (**A**) Scatter plot of an exemplary rate coding unit. For the rate coding analyses, spikes were considered in the period from 0 to 1 s (i.e. the time window of the stimulus) (**B**) Spiking rate (spikes/trial), for each modulation rate, of the example unit shown in **A**. Note the monotonic increase of the firing rate relative to the modulation rate. The Spearman's R of this unit (i.e. the correlation between spiking rate and modulation frequency) was of 0.81 ($p = 4.6x10^{-3}$). (**C**) Normalized spiking rate across the population of rate coding units (n = 12). Note that the firing rate increases with modulation frequencies, particularly in response to periodicities higher than 13.92 Hz. (**D**) Quantification of rate coding units in the groups of trackers (blue) and non-trackers (red). (**E**) Spearman's R of the population of rate coders. High values indicate a strong correlation between firing rate and modulation frequency.

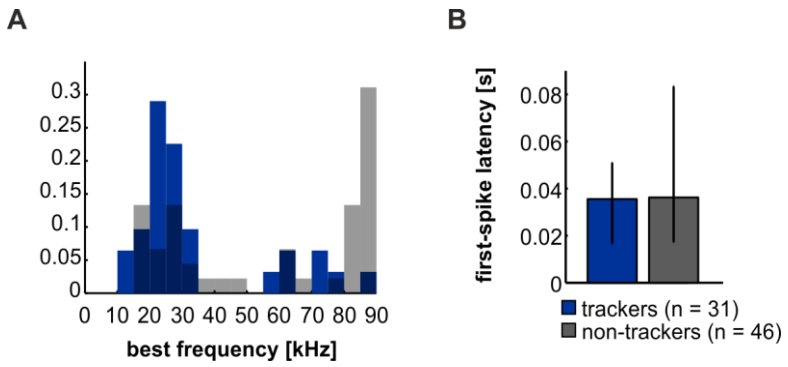

Fig. S3. **Basic properties of tracking and non-tracking units (related to Figures 1 and 3).** (**A**) Distribution of best frequencies (BF, tone frequency at which a unit responded with the most spikes) of tracking (blue histogram) and non-tracking (gray histogram) units. There were significant differences in the BF distribution of trackers and non-trackers (two-sample Kolmogorov-Smirnov test, $p = 0.0019$). (**B**) First spike latency of tracking (blue) and non-tracking (gray; shown as median and quartiles in both cases) units in response to AM stimuli (first spike times were pooled across modulation frequencies). There were no significant differences between the two subpopulations (FDR-corrected Wilcoxon ranksum test, $p = 0.2941$).

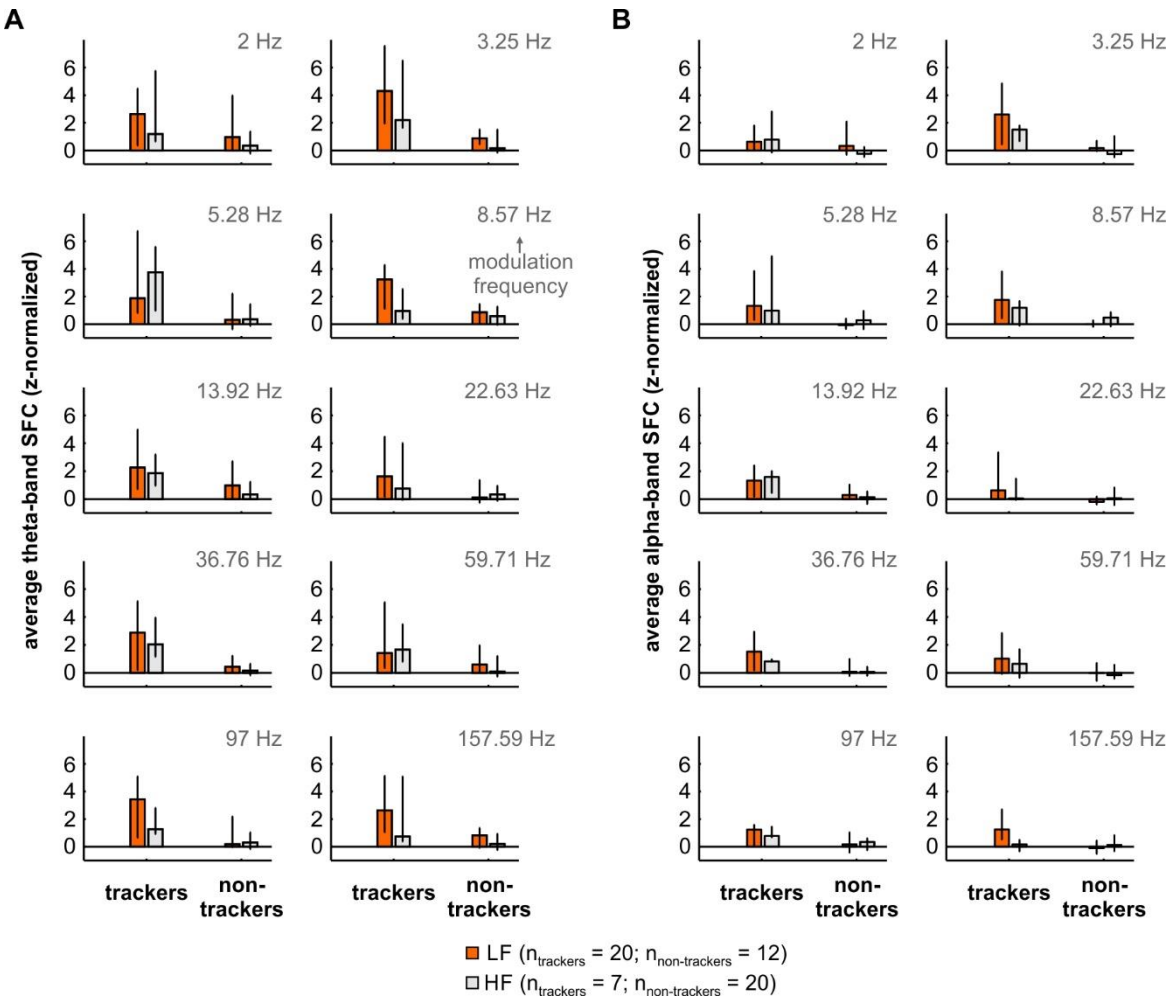

Fig. S4. Spike-field coherence was not significantly different between low and high frequency units (related to Figures 3 and S3). (**A**) Each sub-panel shows the comparison of theta-band z-normalized SFC between low (orange) and high (gray) frequency units within the subpopulation of trackers or non-trackers (left set, or right set, respectively), across modulation rates. Units were deemed as low frequency tuned if their best-frequency was not higher than 50 kHz, and high frequency tuned otherwise, as in previous articles (Esser and Eiermann, 1999; Hagemann et al., 2010; Hagemann et al., 2011). (**B**) Data is shown following the same conventions as in (**A**), but SFC values were compared in the alpha-band (8 – 12 Hz). There were no significant differences in the spike-field coherence of low and high frequency tuned neurons in theta- and alpha-bands (FDR-corrected Wilcoxon ranksum test; corrected $p > 0.066$). The data is shown as median and IQR. Sample sizes are indicated in the figure.

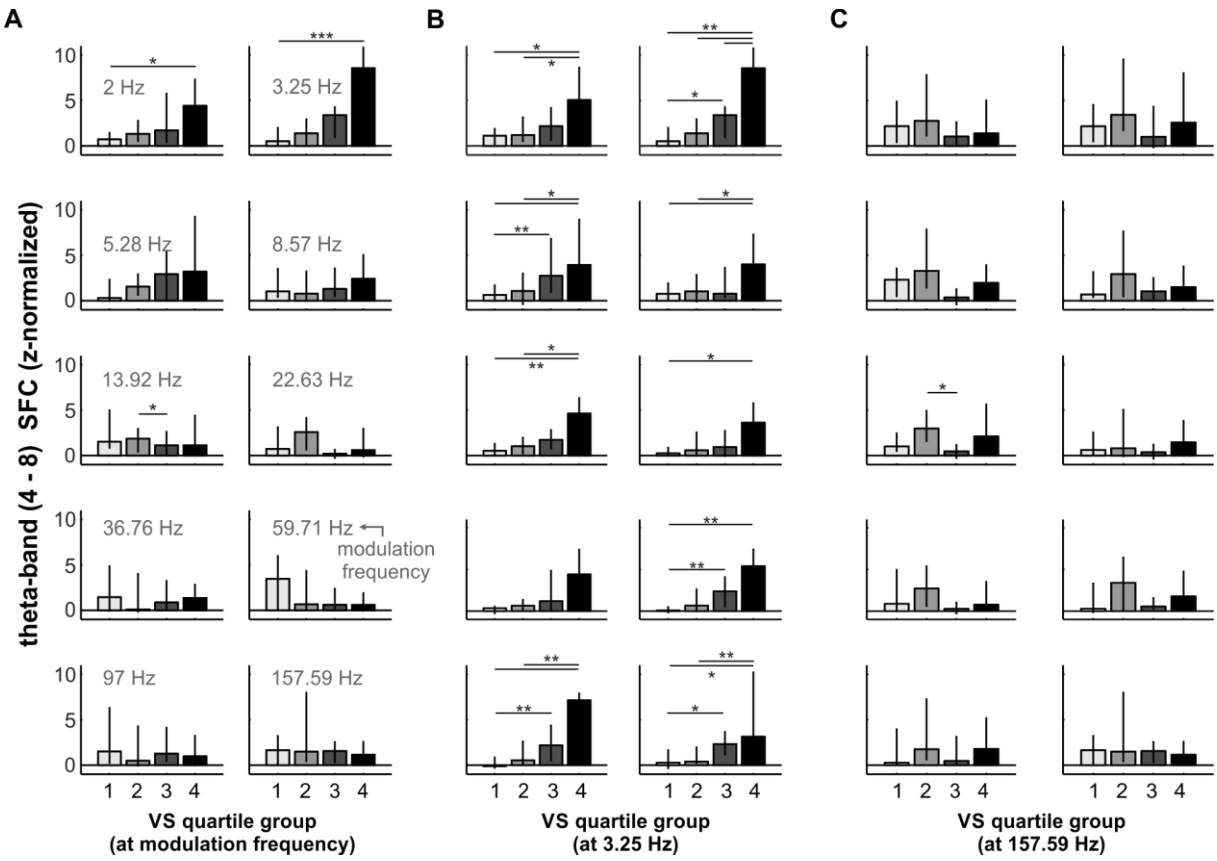

Fig. S5. Theta-band SFC is related to the strength of spike-stimulus synchronization (related to Figure 3). (**A**) Subsets of SFC values across units, divided according to the VS at the modulation frequency under consideration (note that there are four equipopulated subsets, each of n = 17 units; modulation rates are indicated in the plots). VS quartile group 1 contains units with the lowest 25 % vector strength values, whereas group 4 contains units with the highest 25 % vector strength values. The SFC increases together with the VS quartile group, provided that spike-AM synchronization strength is calculated in response to modulation rates < 13.92 Hz. (**B**) Relationship of theta-band spike field coherence, dividing the units into VS quartiles considering spike-stimulus synchronization in response to a modulation rate of 3.25 Hz. Across modulation frequencies, SFC values increased together with VS quartile group. (**C**) Same as in **A** and **B**, but VS values considered were obtained in response to a modulation frequency of 157.59 Hz. Note that there is no relationship between SFC values and VS quartile groups. (significance was assessed with FDR-corrected Wilcoxon rank-sum tests; *, corrected $p < 0.05$; **, corrected $p < 0.01$).

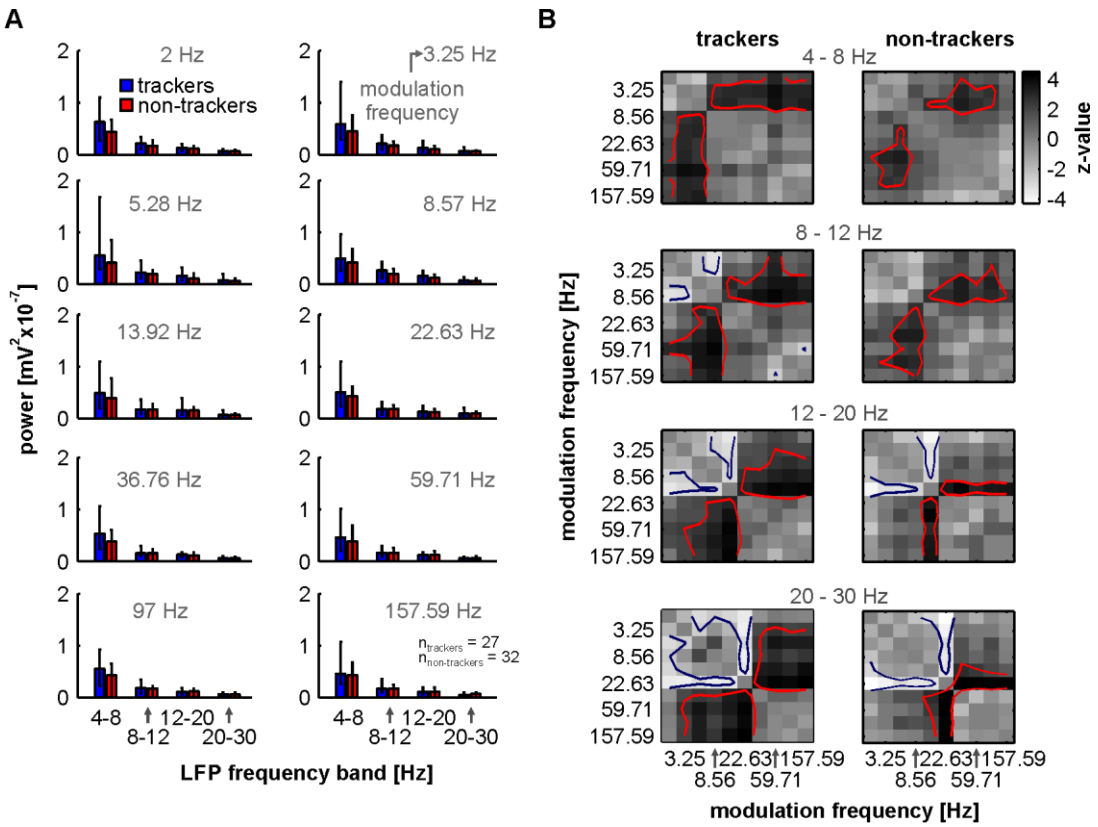

Fig. S6. Power in low frequency bands of the LFP does not explain differences in spike-field coherence (related to Figure 4). (**A**) LFP power in the canonical low frequency bands analyzed in the study, shown for trackers (blue) and non-trackers (red), across modulation frequencies. There were no significant differences in the power of the LFP related to trackers and non-trackers, in any frequency band analyzed (FDR-corrected Wilcoxon ranksum test, $p > 0.06$). (**B**) Each matrix depicts the outcome (z-value) of statistical pairwise comparisons (Wilcoxon signed ranked tests), comparing the power in the LFP of trackers (left column) or non-trackers (right column) in response to each modulation rate. For example, the top-left matrix shows pairwise comparisons of theta-band LFP power (from tracking units) in response to different modulation rates. The value of each cell (i,j) in the matrix is the z statistic obtained by comparing the LFP power in response to modulation frequencies i and j. Red and blue contour lines limit regions of statistical significance (red, power in response to modulation rate i was higher than the power in response to modulation rate j; blue indicates the opposite). The significance threshold was of z = +-2.33 (equivalent to an FDR-corrected p = 0.0198). In the top-matrix it can be observed that the power of theta band LFPs, in trackers, was significantly higher in response to a modulation rate of 3.25 Hz, than in response to modulation rates > 8.56 Hz. Note that, overall, in each neuronal group there were significant differences in the LFP power in response to distinct modulation rates, which also depended on the frequency band under consideration.

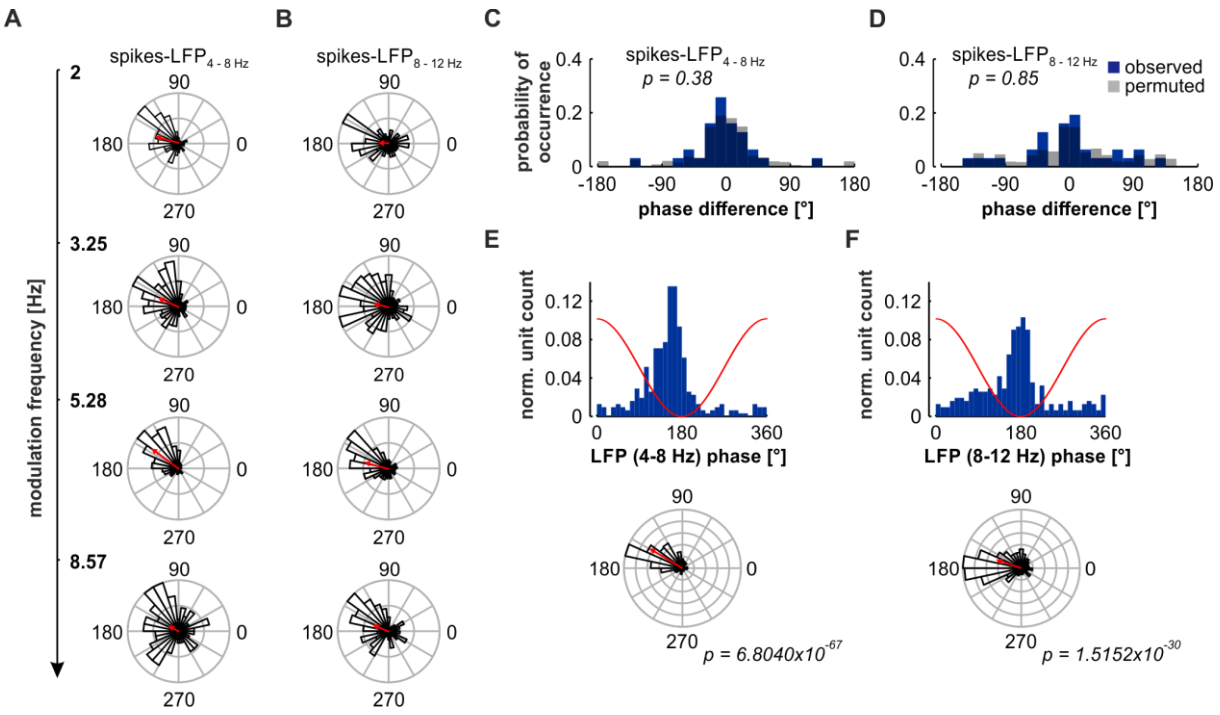

Fig. S7. Robustness of spike-phases relative to theta and alpha bands of the LFP across modulation rates (related to Figure 6). (**A**) *Left column*: spike-phases relative to theta (4 - 8 Hz) band LFPs, across modulation rates, in an example unit (same tracker shown in **Fig. 1**). (**B**) Spike-phases relative to alpha (8 – 12 Hz) band LFPs. Note that the spikes here are the same spikes as in **A**. (**C**) Distribution of spike-phase differences between two consecutive modulation frequencies, when phases were calculated relative to theta LFPs. The observed distribution is shown in blue, whereas a surrogate (randomized differences across not-ordered modulation rates) distribution is shown in gray. There were no significant differences between the randomized and the observed distribution (Fisher's circular mean test, p = 0.38). (**D**) Same conventions as in **C**, but spike-phases were calculated relative to alpha-band LFPs. No significant differences occurred between the observed and the surrogate phase difference distributions (Fisher's circular mean test, p = 0.85). (**E**) Histogram (top) and circular histogram (bottom) for the distribution of preferred spike-phases (relative to theta-band LFPs) in tracking units (n = 31), across all modulation frequencies tested (i.e. each tracking unit and modulation frequency is represented). The red trace in the top histogram illustrates the phase convention relative to the LFP; the red line in the circular histogram shows the mean vector of the phase distribution. Statistics showed that there was a significant directionality in the spike-phases (Rayleigh test for non-uniformity, $p = 6.80 \times 10^{-67}$). (**F**) Same as conventions than panel **E**, but spike-phases were calculated relative to alpha-band LFPs. There was a significant directionality in the spike-phases relative to the alpha oscillations ($p = 1.52 \times 10^{-30}$).

Transparent Methods

Surgical procedures and animal preparation

All experimental procedures were in compliance with current German laws on animal experimentation, and were approved by the Regierungspräsidium Darmstadt (experimental permit #FU-1126). The study was performed on 7 fruit eating bats *Carollia perspicillata* (3 males). Animals were obtained from the colony in the Institute for Cell Biology and Neuroscience of the Goethe University in Frankfurt am Main, Germany.

Before undergoing surgery, the animals were subcutaneously anesthetized with a mixture of ketamine (10 mg * kg^{-1} Ketavet, Pfizer) and xylazine (38 mg * kg^{-1} Rompun, Bayer). Local anesthesia (ropivacaine hydrochloride, 2 mg/ml, Fresenius Kabi, Germany) was subcutaneously applied in the area of the scalp prior to surgery and to any subsequent handling of the wounds. A longitudinal midline incision was made along the skin covering the superior part of the head. Skin and muscle tissues were removed to expose the skull around the region of interest (the AC), such that sufficient area of the bone would remain uncovered to place a custom-made metal rod (1 cm length, 0.1 cm diameter), used to fix the head of the bat during the experimental sessions. The metal rod was attached to the skull using dental cement (Paladur, Heraeus Kulzer GmbH, Germany).

The location of the auditory cortex was determined macroscopically with the aid of previously described landmarks (Esser and Eiermann, 1999; Hechavarria et al., 2016), such as the pseudocentral sulcus and prominent blood vessels in its vicinity. Once located, the AC was exposed by cutting a small hole (roughly of 1 mm^2) in the skull with the aid of a scalpel blade. After surgery, the animals were allowed to rest for at least 2 days before being used for the electrophysiology measurements.

Neuronal recordings were performed chronically in awake bats (no anesthetic was applied on the day of the recording sessions). The experimental sessions lasted for no more than 4 h a day. During recordings, water was offered to the animal at periods of 1 – 1.5 hr. Each bat had at least one day of recovery after each session, and was not used for more than 6 experiments altogether.

Electrophysiological recordings

Experiments were conducted inside a sound-proofed and electrically shielded chamber containing a custom-made holder in which the bat was placed during measurements. The temperature of the holder was kept constant by means of an underlying heating blanket set to

30°C (Harvard, Homeothermic blanket control unit). The speaker (NeoCD 1.0 Ribbon Tweeter; Fountek Electronics, China) used for free-field stimulation was placed inside the chamber, 12 cm away from the bat's right ear, contralateral to the AC in the left hemisphere where recordings were performed. The speaker was calibrated using a $\frac{1}{4}$-inch microphone (Brüel & Kjaer, model 4135, Denmark) connected to a custom-made microphone amplifier.

Electrophysiological data was acquired by inserting a carbon electrode (Carbostar-1, Kation scientific; Impedance at 1 kHz: 0.4 – 1.2 MΩ) into the AC of the left hemisphere of the bat. A silver wire, touching the dura of a non-auditory area of the contralateral hemisphere, was used as reference electrode. The depth of the carbon electrode was accurately controlled from outside of the chamber with a Piezo manipulator (PM-101, Science products GmbH, Hofheim, Germany). Recordings were performed at depths between 300-500 µm from the cortical surface, corresponding to layers III/IV of the primary auditory cortex (AI), although we cannot discard the presence of neurons from the high frequency fields (Esser and Eiermann, 1999). Electrical signals were amplified (Dagan EX4-400 Quad Differential Amplifier, Minneapolis, MN; gain = 100, filter low cutoff frequency = 0.01 Hz, high cutoff frequency = 3 kHz), and underwent an analog-to-digital conversion (RP2.1 Enhanced real time processor, Tucker-Davies Technologies, 2 channel A/D converter, 2 channel D/A converter, 24-bit precision, Alachua, FL) with a sampling rate of 12.2 kHz before being sent to the recording computer via USB, in which the data was stored and online monitored with a custom-written Matlab (version 7.9.0.529 (R2009b), MathWorks, Natick, MA) software.

Acoustic stimulation

Acoustic stimulation was controlled with the custom-written Matlab software that was used for electrophysiological data acquisition (see above). Frequency-level receptive fields were calculated from responses to pure-tone stimuli with a duration of 10 ms (0.5 ms rise/fall time), with randomly selected frequencies ranging from 5 to 90 kHz (5 kHz steps), and sound pressure levels (SPL) from 20 to 80 dB SPL (steps of 10 dB SPL). The SPL of the tones was adjusted online according to the calibration curve of the stimulation speaker, and each frequency-level combination was repeated 5 to 8 times. Based on the frequency receptive fields of the recorded units, it was possible to define a best frequency (BF) / best level (BL) combination to which the unit was most responsive (i.e. the unit fired the highest number of spikes across all pure-tones tested). The BF/BL combination of each unit was used for synthetizing the AM sounds (see below).

Sinusoidally amplitude modulated sounds were generated by multiplying a carrier sinusoid with other slower (modulating) sinusoidal signal. The frequency of the carrier was adjusted to the BF of the unit that was being analyzed, and the SPL of the stimulus was set to be equal to the unit's BL. Modulation frequencies ranged from 2 – 157.59 Hz, increasing in an exponential manner and comprising the following 10 values: 2, 3.25, 5.28, 8.57, 13.92, 22.63, 36.76, 59.71, 97 and 157.59 Hz, with a modulation index of 1. The duration of the AM sounds was set to 1 s, and a linear fading function (10 ms in length, varying from 0 to 1) was multiplied to the beginning and the end of each acoustic stimulus to avoid artefacts during sound presentation. Each AM stimulus was presented for at least 20 repetitions in a randomized order, with a 500 ms inter-stimulus interval, and a pretime per trial (i.e. time lapse between the start of the recording and the stimulus onset) of 10 ms.

All generated sounds were converted to analog signals with a sound card (M2Tech Hi-face DAC, 384 kHz, 32 bit) prior presentation, and sent to an analog power amplifier (Rotel power amplifier, model RB-1050) in order to be presented to the bat through the speaker located inside the chamber (see above for specifications).

Separation of spikes and LFPs

All data analyses were performed off-line with custom-written Matlab (version 8.6.0.267246 (R2015b)) scripts. Spikes and LFPs were separated by digitally filtering the acquired raw signal with a 3rd order band-pass Butterworth filter with cutoff frequencies of 0.1 and 300 Hz for LFPs, and of 300 to 3000 Hz for spikes. Spike detection was based on their amplitude relative to the recording noise baseline, and spike threshold was defined manually for each unit. The spike pattern obtained in response to AM sounds was visualized by means of raster plots and peri-stimulus time histograms (PSTHs) with 1 ms bins.

Trials with motion artefacts were identified offline by looking for large 'pseudo-spikes'. Such pseudo-spikes occurred in long bursts and were higher in amplitude than 'real' spikes. We observed that the set of spike amplitudes in the recorded units followed a gamma-like distribution. With this in mind, we defined a threshold for 'pseudo-spiking events' at the 8th decile (i.e. 80% of the values) of the spike amplitude distribution for a particular unit (including all detected spikes). If a single trial contained more than 10 occurrences of pseudo-spiking events (that is, more than 10 spikes larger than the defined threshold in the 8th decile), such trial was considered as contaminated by motion artefacts and was not used for any subsequent analyses. Thorough visual inspection of raster plots and PSTHs corroborated that the overall response of the units was 'cleaned' of artefacts. If the method failed to 'clean' the

response, or too many trials were lost (> 50%), the unit was not considered for further analyses. In our data, the second case did not occur.

Spike – stimulus synchrony

The synchronization of the spiking activity of cortical units was quantified with the vector strength (VS) metric (Goldberg and Brown, 1969). The VS is a coefficient between 0 and 1 that indicates the strength of synchronicity, and is equivalent to the 'circular mean' of the phase distribution of the spikes relative to the stimulus envelope. It was calculated on a trial-by-trial basis for each modulation frequency, in every unit. In a single trial, the VS was defined as follows:

$$VS = \left|\frac{1}{n}\sum_{k=1}^{n} e^{i\phi_k}\right| \quad (1),$$

where n is the number of spikes fired in that trial, and ϕ_k is the phase of the *k*-th spike relative to the stimulus envelope.

In order to statistically validate the synchronization index provided by the VS values in a particular unit, we conducted a Rayleigh test by pooling all the spikes fired in all trials for every modulation frequency tested. A unit was considered as phase-locked in a certain modulation frequency if it met two criteria: (i) the p-value of the Rayleigh test was lower than 10^{-5}, and (ii) the median VS of the unit at that modulation frequency was higher than the population median in the same frequency. The combination of these criteria is referred as the "joint criterion", and was used to corroborate significant outcomes of the Rayleigh test, which might yield type I errors in specific occasions (Yin et al., 2011). If a unit did not meet the joint criterion in a certain modulation frequency, it was considered as not synchronized to that specific AM.

Additionally, we observed that independently of the modulation frequency tested, most of the units had a strong onset response (heavy burst of spiking activity), lasting up to 70 – 100 ms after stimulus presentation. Therefore, to avoid possible biases in the calculations due to the described onset response, only spikes that occurred past the time mark of 100 ms after stimulus onset were considered for analyses.

Spike – LFP coherence

The spike-field coherence (SFC; (Grasse and Moxon, 2010; Rutishauser et al., 2010)) was used to quantify the synchronization between the spiking activity and the LFP of the recorded units in response to AM sounds. Briefly described, the SFC is a frequency-dependent

coherence index that ranges between 0 and 1, indicating the degree of synchronization (0, for complete lack of synchrony; 1, for perfect synchrony) between action potentials and LFPs.

Conceptually, the method is based on the selection of a number of LFP windows from a longer LFP trace. LFP windows are selected at the times of spike occurrences in a particular neuron. The mean of these windows is termed spike-triggered average (STA). Because of the averaging, the STA maintains only those oscillatory components that are phase-consistent among the considered LFP segments and thus phase-consistent with the spike timings, whereas non-phasic LFP components are 'averaged out'. For calculating the SFC, the power of the STA is normalized by the average of the power spectrum obtained from each individual LFP window analysed. The latter is known as the spike-triggered power (STP). The ratio between the power of the STA and the STP yields a coefficient between 0 and 1 that describes the strength of synchrony depending on the frequency. The SFC can be expressed as follows:

$$SFC(f) = \frac{\Psi(\mathrm{STA})}{\frac{1}{n}\sum_{i=1}^{n}\Psi(w_i)} \qquad (2),$$

where $\Psi(\cdot)$ is the function used for obtaining the power spectrum, and the denominator is the STP of a series of LFP windows $w_{1,2,3,\ldots,n}$. The spectrum obtained when calculating coherence values is referred to as coherence spectrum.

Because the SFC metric is sensitive to the number of spikes used for its calculation (Grasse and Moxon, 2010), we used only those units that fired a minimum of 40 spikes in response to each modulation frequency tested. Since individual trials in our data were unlikely to contain that amount of spikes, we pooled the spikes belonging to all the trials of the same modulation frequency tested in a particular unit, and selected randomly 40 of them to use as centers for the LFP windows. Note that this implies that if there is consistent phase coherence between spikes and LFPs, it will be maintained across trials. The random selection of 40 spikes was repeated 300 times in order to reduce sampling effects, yielding an equal number (300) of SFC curves for each unit and modulation frequency. The median of these curves was considered as the SFC in the modulation frequency for the unit under consideration.

The LFP windows used for SFC computations were chosen to spread $\pm$ 200 ms from the time of spike occurrence, and only spikes for which their windows' edges fit in the time lapse of 100-1000 ms after stimulus onset were considered. The power spectra of the LFP segments were obtained with the multitaper method (Percival and Walden, 1993), available in the Chronux toolbox (Bokil et al., 2010), using 2 tapers with a time-bandwith (TW) product of 2. All power spectra in the manuscript were calculated with the same parameters.

To compare values of SFC against those that would occur by chance, we calculated a reference baseline by destroying spike-related phase synchrony across LFP segments chosen from trials belonging to a specific modulation frequency. The baseline was constructed by selecting 40 LFP windows (same number of segments used to calculate the SFC) centered at random time points, such that the windows' edges were not more extreme than times of 100 or 1000 ms after stimulus onset (same as above). The same analyses used for computing the SFC (see preceding text) were applied to these windows, yielding a baseline SFC in which values of phase coherence for this unit were disassociated from actual spike times. This procedure was repeated 300 times, rendering the same number of baseline SFC curves. Note that the same window length, number, and spectral analysis used for obtaining the SFC were used to obtain the baseline. In the manuscript, we refer to the averaged LFP windows used for baseline calculations as random-triggered average (RTA), to the average power of such windows as the random-triggered power (RTP), and to the corresponding field coherence as random-field coherence (RFC). This nomenclature was defined in a way that relates to terms such as STA, STP, and SFC, while still allowing to differentiate spike-centered and randomized coherence metrics.

The median SFC value of each unit, across modulation frequencies, was z-normalized to the corresponding RFC (i.e. the baseline distribution of SFC values). The z-normalized SFC was used to compare statistically coherence values between tracking and non-tracking units. Statistics were performed comparing the mean z-normalized SFC in canonical LFP bands (theta, 4 - 8 Hz; alpha ,8 – 12 Hz; low beta, 12 – 20 Hz; and high beta, 20 – 30 Hz), between tracking and non-tracking units, with FDR-corrected (Benjamini and Hochberg procedure; (Benjamini and Hochberg, 1995)) non-parametric Wilcoxon ranksum tests.

LFP – stimulus coherence

To address the synchronization between LFPs and the stimulus' envelope we extended the SFC approach into a slightly different metric: the stimulus-field coherence (StimFC). The principle behind this metric is clearer when considering the envelopes of the presented AM sounds as well defined periodic and phasic events. With this in mind, it is possible to quantify the phase-locking of the LFP to the stimulus' envelope by selecting a series of windows, each related to the same time point (i.e. a particular trough, a valley, or any desired phase of the envelope), across test trials of the same modulation frequency. The average of these windows is then the stimulus-triggered average (StimTA), and the mean power spectrum would be the stimulus-triggered power (StimTP). Note that, as it occurs with the STAs, only phase-

consistent oscillatory events will remain after the averaging is performed. Similar to the SFC, the StimFC is calculated as follows:

$$StimFC(f) = \frac{\Psi(\,\mathrm{StimTA}\,)}{\frac{1}{n}\sum_{i=1}^{n}\Psi(\,w_i\,)} \quad (3),$$

where the symbols indicate the analogous values to eq. (2). The only difference is that for the StimFC calculation, LFP windows are not chosen around spike times, but related to a particular time point of interest relative to the stimulus onset.

The nature of the approach makes the StimFC metric sensitive to the number of windows used. To quantify coherence between LFP and stimulus' envelopes across modulation frequencies, we sacrificed unit specificity in order to bring power to the method by increasing the amount of considered windows. Per modulation frequency, a total of 300 LFP segments (900 ms long) starting at 100 ms after stimulus onset, were randomly chosen from a pool that included all the trials from the units tested in the modulation frequency of interest (either tracking units or non-tracking units at once). Although unit specificity was lost, this approach allowed us to address whether the non-simultaneously recorded LFPs in different sites of the auditory cortex (across electrode penetrations), and even different animals, still exhibited some degree of synchronization related to the stimulus envelope. Note that after averaging across units and trials, synchronized oscillatory patterns will appear only if they are triggered by (and related to) the stimulus, while being independent of the unit they were related to, or the animal from where they came. The selection of 300 random segments was repeated 500 times, and each StimFC curve was used for further comparisons.

In a similar manner, baseline StimFC values were computed per modulation frequency by randomly selecting LFP windows (n = 300, spanning 100 – 1000 ms after stimulus onset; 500 repetitions) from the same 'pooled' trials that were used for the StimFC calculations. However, each selected window was split at a random time point, and the resulting parts of the LFP segment were swapped. Note that this effectively destroys phase consistencies between the segments and the AM envelope, and thus allows to calculate surrogate coherence estimates. As with the SFC analyses (see above), observed StimFC values were z-normalized to such surrogate StimFC, on a modulation rate basis.

Modulation of the low-frequency LFP amplitude by the stimulus phase

Phase-amplitude coupling (PAC) analyses were performed as described in (Tort et al., 2010). We focused on the modulation of the amplitude of low-frequency LFPs by the phase of the

stimulus' envelope, mainly because SFC differences were observed in the theta-alpha range. For this, LFPs were filtered in the canonical low-frequency bands (theta, alpha, low beta, and high beta) and their instantaneous energy $A(t)$ was calculated by means of the absolute value of the Hilbert transform. The phase component used for the PAC calculations was obtained from the stimulus envelope. The instantaneous phase $\phi(t)$ of the stimulus was readily available since it was an artificially generated AM sound. With both the instantaneous stimulus phase and LFP energy, we defined a composite time series $[\phi(t), A(t)]$, which relates the amplitude of the LFPs to each phase of the envelope. We then binned the phases into 36 equi-populated bins (10° bin size) and defined for each bin *j* a value equal to the mean LFP instantaneous energy, $A(t)$, for phases that fell within that particular bin. The amplitude of each bin was later normalized dividing the value of each bin by the sum of the values across all bins, which results in a distribution that holds the properties of a discrete probability density function (pdf). This is referred to as the "amplitude distribution" (Tort et al., 2010).

A Modulation Index (MI) was calculated by contrasting the observed amplitude distribution across phases with a random uniform (null) distribution. In this case, such null distribution reflects what would occur if the fluctuations of power in a certain LFP band would not be related to the phase of the stimulus. The MI quantifies how different the observed amplitude distribution and the null distribution are by normalizing the Kullback-Leibler (KL) distance (Kullback and Leibler, 1951), thus yielding values between 0 and 1 (0, no modulation; 1, perfect modulation). The MI was calculated as follows:

$$MI = \frac{D_{KL}(P,U)}{\log_2 N} \qquad (6)$$

where $D_{KL}(P,\ U)$ is the KL distance between the amplitude distribution (P) and the null distribution (U), and N stands for the number of bins. In order to obtain a uniform distribution, we generated 10000 uniformly distributed random numbers ranging from 1 to 36 (the number of bins used), and counted how many times a particular bin appeared in the list of random numbers. MIs were calculated for both tracking and non-tracking units (always using the same null distribution), and were then compared across modulation frequencies via non-parametric Wilcoxon ranksum tests. Statistical significance was accepted for p-values below an FDR-corrected (Benjamini and Hochberg procedure) threshold. Note that to avoid possible biases caused by onset responses, analyses were performed on envelope segments starting at the first trough past 100 ms after stimulus onset.

Inter-trial coherence

The consistency of the instantaneous phase of low frequency LFPs across trials was quantified by calculating the inter-trial coherence (ITC) metric. For each unit and modulation frequency, LFP traces were filtered according to the frequency band under consideration (4th order Butterworth filter), and their instantaneous phase was extracted by means of the Hilbert transform. Let $\phi(k,t)$ be the instantaneous phase of the filtered LFP at time *t* and trial *k*, of a particular unit in response to a certain modulation frequency. The ITC at time point *t* can be calculated according to:

$$ITC(t) = \left|\frac{1}{N}\sum_{k=1}^{N} e^{i\phi(k,t)}\right| \quad (7),$$

where N represents the number of trials. The ITC ranges between 0 and 1, indicating the strength of the phase consistency of the LFP across trials.

ITC values corresponding to the subpopulations of tracking and non-tracking units were compared across modulation frequencies, by subtracting the median ITC of the subpopulation of trackers minus the median ITC of the subpopulation of non-trackers, for every modulation rate tested. Throughout the text, we refer to this difference as the ITC difference (dITC). A surrogate dITC was generated by randomly permuting labels ("trackers", "non-trackers") of units, and recalculating the same differences between randomly labeled subpopulations, for each modulation frequency. This randomization procedure was repeated 2500 times, yielding a surrogate distribution of differences at each modulation rate, in which the actual differences between neuronal groups were minimized to chance level. Because of the large number of repetitions, for computational purposes the ITC data was down-sampled from 12.2 kHz (sampling frequency of the recording device) to 200 Hz. The dITC was z- normalized to the surrogate distribution, and the z-normalized values were used as a measure of significance, with an uncorrected threshold set at z = 1.96 (equivalent to a p-value of 0.05). Positive z-normalized dITC values indicate higher ITC in trackers than non-trackers, while negative values indicate the opposite.

Relationship between spiking, phase of the AM stimuli, and low-frequency LFPs

In order to explore the phase relation between neuronal firing and AM stimuli in the recorded units, a phase related to the AM envelope was assigned to each spike in the same way as it was done for VS calculations. As mentioned in the preceding text, spikes were only considered when they occurred in the time window between 100-1000 ms after stimulus presentation, thus avoiding onset and offset responses that could bias the calculations. The

distributions of stimulus phases at which the units fired their spikes were plotted as circular histograms for each modulation frequency. Preferred stimulus phases were obtained by calculating the phase of the mean orientation vector of the circular distribution in each unit and modulation frequency. Units were only considered for the preferred phase calculations if they fulfilled the joint criterion for the particular AM frequency under study (note that this implies that only trackers were used). The preferred AM phase of the units was studied only for the six slowest AM frequencies tested (i.e. from 2 to 22.63 Hz), as those are the frequencies most cortical neurons are capable of locking their spikes to (Martin et al., 2017).

To test for differences in the preferred phase, across modulation frequencies, the angular difference between mean orientation vectors obtained from two distinct modulation rates was calculated based on trigonometric relationships relying on the cross and the dot products between the vectors, considering that:

$$tan\phi = \frac{sen\phi}{cos\phi} = \frac{||u \times v||}{u \cdot v} \qquad (8),$$

where ϕ is the angle between vectors *u* and *v*, and $||u \times v||$ indicates the norm of the cross product between these vectors, while $u \cdot v$ stands for the dot product between them. The angle ϕ is measured in the counterclockwise direction, and a positive sign indicates a counterclockwise rotation from *u* to *v*, with an equivalent angle. In this case, vectors *u* and *v* can be thought as the mean vectors of two different modulation rates.

The effect of raising the modulation frequencies on the spike phase was quantified by calculating angular differences within each unit, between the phase of the mean orientation vectors obtained in response to two successive AM rates (a lower and a higher rate). The above was only done for pairs of modulation frequencies to which the unit was significantly synchronized, according to the joint criterion (modulation rates were chosen in such way that their values would be as close as possible). The set of differences obtained would be centered at zero, if overall the units would not change preferred phases as the presented envelopes increased in frequency. On the other hand, a shift towards positive phase differences would indicate a phase lag (the units tend to respond to a later envelope phase as modulation frequencies increase), whereas a shift towards negative phase differences would suggest a phase acceleration (the units tend to respond to an earlier phase of higher AM envelopes).

To assess statistically the presence of an effect caused by an increase of the stimulus modulation frequency, a randomization test was performed to generate a null distribution testing the hypothesis that the increase in the stimulus modulation rate does not account for

the observed distribution of phase differences. For each unit, mean vectors calculated in response to different modulation rates were randomly paired (if the unit satisfied the joint criterion in those modulation rates), and their angular difference was obtained. Such a procedure was repeated 10000 times, and the surrogate distribution carrying no effect of orderly increasing the modulation frequencies was statistically compared with the observed distribution using a nonparametric circular test for equal medians (Fisher's circular median test, threshold of $p = 0.05$).

We performed similar analyses to test whether the change in modulation frequency would affect predictably the synchronization of the spikes and the low frequency LFP bands. For each unit, we obtained the preferred spike-phase relative to low frequency LFPs (in the bands of 4 – 8, 8 – 12, or 4 - 12 Hz; 4^{th} order Butterworth filter), only considering modulation frequencies in which the unit satisfied the joint synchronization criterion. The instantaneous phase of the LFP was calculated from the Hilbert-transformed low frequency LFP.

Phase differences were obtained as described for the preferred AM phases (see preceding text), across (ordered) modulation rates. As mentioned above, a phase difference distribution centered at 0 degrees, shifted towards positive angles, or shifted towards negative angles, would indicate no phase change, a phase lag, or a phase acceleration, respectively. A randomization test similar to the one described in the preceding text was used to generate a surrogate distribution of phase differences, in which there was no effect of changing the modulation rate of the stimulus in an orderly manner (i.e. increasingly or decreasingly). The observed and randomized distributions were then statistically compared by means of a Fisher's circular median test (significance threshold at $p = 0.05$).

Supplementary references:

Benjamini, Y., and Hochberg, Y. (1995). Controlling the False Discovery Rate - a Practical and Powerful Approach to Multiple Testing. J Roy Stat Soc B Met *57*, 289-300.

Bokil, H., Andrews, P., Kulkarni, J.E., Mehta, S., and Mitra, P.P. (2010). Chronux: a platform for analyzing neural signals. Journal of neuroscience methods *192*, 146-151.

Esser, K.H., and Eiermann, A. (1999). Tonotopic organization and parcellation of auditory cortex in the FM-bat Carollia perspicillata. Eur J Neurosci *11*, 3669-3682.

Goldberg, J.M., and Brown, P.B. (1969). Response of binaural neurons of dog superior olivary complex to dichotic tonal stimuli: some physiological mechanisms of sound localization. J Neurophysiol *32*, 613-636.

Grasse, D.W., and Moxon, K.A. (2010). Correcting the bias of spike field coherence estimators due to a finite number of spikes. J Neurophysiol *104*, 548-558.

Hagemann, C., Esser, K.H., and Kossl, M. (2010). Chronotopically organized target-distance map in the auditory cortex of the short-tailed fruit bat. J Neurophysiol *103*, 322-333.

Hagemann, C., Vater, M., and Kossl, M. (2011). Comparison of properties of cortical echo delay-tuning in the short-tailed fruit bat and the mustached bat. J Comp Physiol A Neuroethol Sens Neural Behav Physiol *197*, 605-613.

Hechavarria, J.C., Beetz, M.J., Macias, S., and Kossl, M. (2016). Vocal sequences suppress spiking in the bat auditory cortex while evoking concomitant steady-state local field potentials. Sci Rep *6*, 39226.

Kullback, S., and Leibler, R.A. (1951). On Information and Sufficiency. Ann Math Stat *22*, 79-86.

Martin, L.M., Garcia-Rosales, F., Beetz, M.J., and Hechavarria, J.C. (2017). Processing of temporally patterned sounds in the auditory cortex of Seba's short-tailed bat,Carollia perspicillata. Eur J Neurosci *46*, 2365-2379.

Percival, D.B., and Walden, A.T. (1993). Spectral analysis for physical applications (cambridge university press).

Rutishauser, U., Ross, I.B., Mamelak, A.N., and Schuman, E.M. (2010). Human memory strength is predicted by theta-frequency phase-locking of single neurons. Nature *464*, 903-907.

Tort, A.B., Komorowski, R., Eichenbaum, H., and Kopell, N. (2010). Measuring phase-amplitude coupling between neuronal oscillations of different frequencies. J Neurophysiol *104*, 1195-1210.

Yin, P.B., Johnson, J.S., O'Connor, K.N., and Sutter, M.L. (2011). Coding of Amplitude Modulation in Primary Auditory Cortex. Journal of Neurophysiology *105*, 582-600.